UPPSALA
UNIVERSITET

Human adenovirus type 5 infection alters mitochondrial membrane dynamics

Erik Schubert

Master Degree Project in Infection Biology, 45 credits. Spring 2021
Department: Medical Biochemistry and Microbiology, Uppsala University
Supervisor: Tanel Punga

Table of Contents

Abstract

Mitochondria are double-membrane organelles that orchestrate essential cellular functions including ATP synthesis, calcium homeostasis and apoptosis. Furthermore, mitochondria are effective stimulators of the innate immune system through the release of mitochondrial components into the cytosol. One such stimulus is mitochondrial DNA (mtDNA) which is recognized by receptors of the innate immune system, such as cGAS or TLR9 due to its resemblance to bacterial DNA. Several viruses have been shown to induce the release of mtDNA, including influenza virus and dengue virus. This thesis utilizes biochemical, qPCR and microscopy methods to study how human adenovirus type 5 (HAdV-C5) infection alters mitochondrial DNA and membrane dynamics. Results in this thesis reveal that also HAdV-C5 induces release of mtDNA into the cytosol, correlating with the expression of a specific viral structural protein during the late phase of infection. Notably, transient transfection of this viral protein is sufficient to release mtDNA into the cytosol. The viral protein harbors an amphipthatic helix whose putative functions are targeting of the viral protein to the mitochondria and altering the mitochondrial membrane integrity. Elimination of the Bax and Bak proteins reduces the viral protein-mediated mtDNA release. In addition, accumulation of the viral protein in mitochondria leads to the hyperpolarization of the inner mitochondrial membrane. Collectively, this thesis reveals novel interactions of HAdV-C5 infection with mitochondrial functions.

Popular Scientific Summary

Mitochondria are the powerhouse of the cell. They earned this title by being responsible for 90 % of the energy production in our cells. In addition, mitochondria are important for controlling cell death if cells encounter high levels of stress. Interestingly, mitochondria contain their own DNA that acts as a blueprint for proteins involved in the mitochondrial energy production system. Research has shown that this mitochondrial DNA can function as a danger signal for our immune system when released into the cell.

Many viruses manipulate mitochondrial functions for their own advantage. For example, viruses can prevent mitochondria from inducing cell death in order to survive within the host cell. However, some viruses such as influenza virus have been shown to stimulate the release of mitochondrial DNA (mtDNA) into the cell. This mtDNA can then activate the immune system to fight the virus infection.

Recent research has found that another well-known virus, the human adenovirus stimulates the release of DNA from mitochondria. Yet, it remains unclear how adenoviruses can cause this release. Therefore, this thesis aims to find out how one of the adenovirus structural proteins is involved in the virus stimulated mtDNA release.

To confirm that human adenovirus causes mtDNA release from mitochondria, cells were infected with the virus. Analysis of different cellular contents showed that in adenovirus infected cells more mtDNA was present outside of mitochondria than in non-infected cells. In order to study the role of the adenovirus-structural protein, an experimental model system was used where the protein alone was introduced into the cells. The cells containing the protein were then analyzed for the presence of mtDNA outside of mitochondria. The results of this thesis show that the viral structural protein by itself was enough to stimulate the release of mtDNA from mitochondria. Furthermore, microscopy images visualized that the viral structural protein localizes to mitochondria.

In future perspectives it would be important to determine how adenovirus induced mtDNA can contribute to the activation of the immune system. Additionally, it would be interesting to investigate if mtDNA release can be beneficial for virus growth. Taken together, this thesis revealed one particular viral protein that is important for the release of mtDNA during adenovirus infection.

Introduction

Background to Mitochondria

Mitochondria are bean shaped organelles that orchestrate essential functions of eukaryotic cells. Structurally, mitochondria are enclosed of an outer and inner membrane with infoldings known as cristae. The inner most compartment of mitochondria is known as the matrix, which contains the mitochondrial DNA, metabolic enzymes and ribosomes (Figure 1) (Campbell and Reece, 2015). Although initially deemed controversial, mitochondria are believed to have evolved from an integrated endosymbiotic proteobacterium during the evolution of eukaryotic cells (Roger et al., 2017). The mitochondrial structure, fusion and fission systems as well as the existence of mitochondrial DNA (mtDNA) support this theory for the mitochondrial origin (Boguszewska et al., 2020). On average, an animal cell contains hundreds to thousands of mitochondria that make up approximately 1/5 of the cells volume (Alberts, 2008). Importantly, mitochondria account for 90 % of the energy produced in a cell, which makes them commonly known as the "powerhouse of the cell" (Siekevitz, 1957). In addition, mitochondria are involved in calcium homeostasis, cell death and innate immune activation (Osellame et al., 2012). Interestingly, mitochondria can dynamically fuse and divide by utilizing the previously mentioned fusion and fission systems. This allows mitochondria to adaptively mitigate stress, remove damaged mitochondria and adjust energy production (Youle and van der Bliek, 2012). On the other hand, mitochondrial impairments can also be linked to various diseases including diabetes mellitus, mitochondrial myopathies and neurogenerative diseases. The most common causes for these diseases are mutations in nuclear or mitochondrial DNA that lead to metabolic dysfunction (Chinnery, 1993; Gorman et al., 2016).

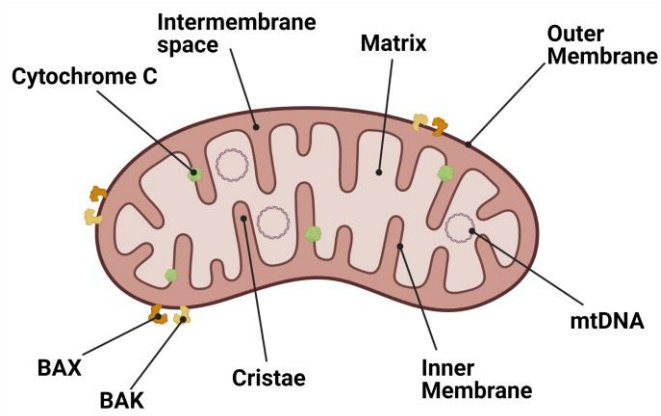

Figure 1. A simplified overview a mitochondrion depicting the main structural components and the localization of the Bax/Bak proteins, cytochrome C and mtDNA.

Mitochondria and its functions

Mostly, mitochondria are known for the production of energy in the form of adenosine triphosphate (ATP) through the process of oxidative phosphorylation (Cooper, 2000). In this process, electrons derived from NADH or $FADH_2$ are passed through several complexes that build up the electron transport chain. The decrease in free energy produced from the passage of electrons is coupled to the pumping of protons from the mitochondrial matrix to the intermembrane space. The energy from the resulting proton gradient is used to drive the synthesis of ATP as protons flow back to the mitochondrial matrix (Cooper, 2000). Apart from energy production, mitochondria have an essential role in programmed cell death (apoptosis). The latter is controlled by mutual interplay between the proteins belonging to the Bcl-2 protein superfamily (Li and Dewson, 2015). This well-described protein family includes both pro-apoptotic (e.g., Bax and Bak) and anti-apoptotic (e.g., Bcl-2) proteins. Cell stress inducers such as genotoxic drugs, gamma radiation or

pathogenic insults trigger the activation and oligomerization of the pro-apoptotic Bcl-2 proteins Bax and Bak, which are located on the outer mitochondrial membrane (Figure 1). Oligomerization of these proteins generates pores that induce mitochondrial outer membrane permeabilization (MOMP) allowing the release of cytochrome C into the cytosol. Consequently, cytochrome C associates with the protein APAF1. This interaction, in turn induces apoptosis through activation of effector caspases (Kalkavan and Green, 2018).

Mitochondrial DNA and the innate immune response

Recent research has also connected mitochondrial components to the stimulation of innate immune responses (West et al., 2011). One such immune stimulus is mitochondrial DNA (mtDNA) that mitochondria have retained from their endosymbiotic ancestors (Ladoukakis and Zouros, 2017). Mitochondrial DNA, which exists as a circular double-stranded DNA (dsDNA), is comprised as nucleoids that reside in the mitochondrial matrix (Figure 1) (Riley and Tait, 2020). With an approximate size of 16.5 kb, mtDNA codes for 21 proteins that are part of the electron transport chain, as well as 2 rRNAs and 22 tRNAs (Lee and Han, 2017). Importantly, mtDNA released from mitochondria is seen as a "foreign" damage associated molecular pattern (DAMP) due to distinct DNA methylation motifs that resemble those of bacterial DNA (Boguszewska et al., 2020). Thus, numerous pattern-recognition receptors (PRRs) can be activated by mtDNA present in an extra mitochondrial milieu (Rodríguez-Nuevo and Zorzano, 2019). Cyclic guanosine monophosphate-adenosine monophosphate (cGAMP) synthase (cGAS) is an example of a PRR that recognizes foreign cytosolic dsDNA such as mtDNA (Verrier and Langevin, 2021). Upon activation, cGAS catalyzes the production of cGAMP which in turn binds the stimulator of interferon (IFN) genes (STING) to induce expression of type 1 IFN genes (Riley and Tait, 2020). Another PRR sensing dsDNA is the toll-like receptor 9 (TLR9) which resides in endosomes of immune cells (Lamphier et al., 2006). Upon activation, TLR9 receptors stimulate a pro-inflammatory response mediated by MyD88 signaling (Martínez-Campos et al., 2017). In addition, oxidized fragments of mtDNA can also promote the activation of NLRP3 inflammasomes (Shimada et al., 2012).

Mitochondrial DNA and viruses

The release of mtDNA from mitochondria can occur as a consequence of endogenous processes, oxidative stress or through various pathogenic insults (Tiku et al., 2020). The aforementioned Bax- and Bak-induced MOMP is one example on how mitochondrial factors such as mtDNA can leak out into the cytosol and trigger the innate immune response (McArthur et al., 2018). Notably, viral infections can be linked to the modulation of mitochondrial functions including the interaction with or release of mtDNA (Anand and Tikoo, 2013). For instance, the herpes simplex virus 1 (HSV-1) encoded UL12 DNase directly targets and degrades mtDNA (Corcoran et al., 2009). In contrast to DNA viruses such as HSV-1, mostly RNA viruses have been associated to the release of mtDNA, noteworthily influenza A (IAV), dengue and severe fever with thrombocytopenia syndrome (SFTS) virus (SFTSV) (Moriyama et al., 2019; Sun et al., 2017; Li et al., 2020). Interestingly, these viruses deploy different mechanisms that lead to mitochondrial membrane disruption. IAV utilizes the virus encoded M2 protein, a proton selective ion channel also known as a viroporin. The M2 protein is essential for IAV envelope disassembly and in turn, escape of the viral RNA from endosomes during virus entry (Cady et al., 2009). Furthermore, M2 has been shown to interact with the mitochondrial antiviral signaling protein (MAVS), triggering a substantial release of mtDNA (Moriyama et al., 2019). The IAV induced mtDNA activates both a cGAS-STING and inflammasome mediated innate immune response (Moriyama et al., 2020, 2019). SFTSV on the other hand, significantly upregulates Bak in a virus infection context (Li et al., 2020). Upregulation of Bak results in enhanced Bax- and Bak-regulated MOMP causing inner membrane herniation and subsequent release of mtDNA (Li et al., 2020). Nevertheless, little is still known about the exact mechanism that different RNA viruses employ

to influence mtDNA. Recently, Mun. 2019 has shown that also a well-known DNA virus, namely human adenovirus C5 (HAdV-C5), can induce mtDNA release into the cytosol of virus infected cells (Mun, 2019).

Human adenoviruses (HAdV)

Human adenoviruses (HAdVs) are linear double-stranded DNA viruses commonly causing upper respiratory tract infections. Due to their wide cell tropism, HAdV infection can also lead to diseases such as conjunctivitis and gastroenteritis (Khanal et al., 2018). Although usually self-limiting, HAdVs can cause serious infection or even death in immunocompromised patients (Hierholzer, 1992). Notably, adenoviruses (AdVs) are important tools to study molecular biological processes such as RNA splicing (Berk, 2016). In addition, AdVs can be selectively engineered to strictly target and kill cancer cells (Garcia-Moure et al., 2017). Furthermore, AdV based vector vaccines have been pivotal in the fight against the present SARS-CoV-2 pandemic (García-Montero et al., 2021).

Human adenoviruses and mitochondria

The genome of HAdVs is approximately 30-36 kb in size and codes for up to 50 proteins, some of which exhibit functions that interfere with mitochondrial processes and could potentially be linked to mitochondrial DNA or membrane dynamics (Acheson, 2011). In particular, the early E1B-19k protein is recognized as the viral Bcl-2 (vBcl-2) homologue with a potent anti-apoptotic function (Han et al., 1996). In the HAdV lifecycle, E1B-19k is essential as it binds and sequesters cellular Bax and Bak preventing MOMP and therefore apoptosis, to promote undisrupted virus replication (Berk, 2005). Another viral protein that to associates with mitochondria is the core-capsid bridging protein V (pV). The main function of pV is to provide stability to the viral capsid by acting as a bridge between the core and other capsid proteins (Ugai et al., 2012). Interestingly, pV has been shown to interact with the mitochondrial p32, a protein which is connected to oxidative phosphorylation, hence ATP production (Matthews and Russell, 1998; Muta et al., 1997). However, the consequence of this interaction has not yet been elucidated. Although HAdV encode proteins that interrelate with mitochondrial components, it has remained unclear what viral factor is responsible for the previously mentioned virus induced mtDNA release. Mun. 2019 has mainly investigated the correlation of the viral pre-histone-like capsid protein VII (pVII) with mtDNA dynamics, but concluded that pVII per se is not sufficient in releasing mtDNA into the cytosol (Mun, 2019).

Human adenovirus protein pVI

As mtDNA release can be linked to mitochondrial membrane disruption, one protein expressed by HAdV comes into question, the late viral capsid protein VI (pVI, also known as pre-cursor protein VI or endosome lysis protein VI). Inside the virus capsid, pVI acts as a stabilizing cement protein by interconnecting the interior capsid proteins with the hexon trimers (Wiethoff and Nemerow, 2015). Based on available data, the pVI protein exists in two forms: the so-called pre-cursor form (amino acids 1-250) and the mature form (amino acids 34-239) which is integrated into the viral capsid (Figure 2). The mature form is produced through pre-cursor protein cleavage by the adenovirus protease (AVP). This site-specific cleavage releases 33 amino acid and 10 amino acid peptides from the N and C terminus of the protein, respectively (Figure 2). Further, the C-terminal peptide functions as a co-factor for the AVP, since this protein is needed for the proteolytic cleavage of several other viral proteins to achieve proper virion maturation (Hernando-Pérez et al., 2020).

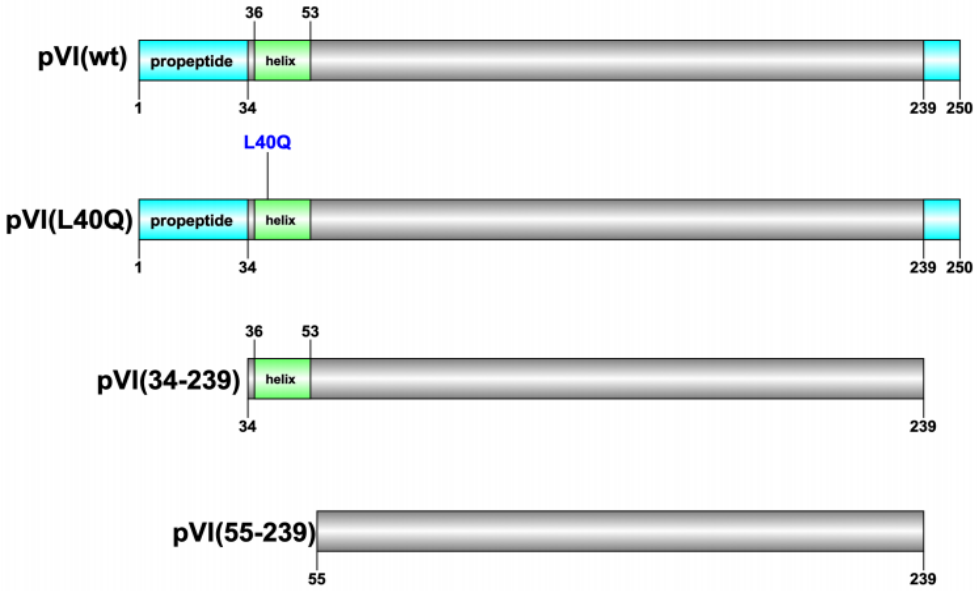

Figure 2. A simplified overview of the HAdV-5 pVI protein. Both pro-peptides, which are cleaved off by the AVP, are indicated in light blue. The amphipathic helix is indicated in light green. Numbers indicate amino acids. L40Q is a point mutation within the amphipathic helix.

Notably, pVI plays a critical role in endosomal membrane lysis during virus entry. Upon uptake in clathrin-coated pits, initiated by the interaction of the viral fiber protein with the coxsackievirus and adenovirus receptor (CAR), the virion is transported to endosomal vesicles (Zhang and Bergelson, 2005). It is crucial for the virion to escape the endosome to ensure continued transport of the viral DNA to the nucleus. Acidification of the endosome triggers virion disassembly and release of pVI from the virion's interior (Zhang and Bergelson, 2005). The endosomal escape of HAdV is mediated by a membrane lytic amphipathic helix located at the N-terminus of pVI (Figure 2) (Wiethoff and Nemerow, 2015). The amphipathic helix allows the protein to anchor itself into the endosomal membrane, and induce a severe positive or negative membrane curvature ultimately leading to membrane fragmentation in a pH independent manner (Figure 3) (Wiethoff and Nemerow, 2015). Feasibly, the membrane disruptive attribute of pVI could also be associated to other membrane structures, including the mitochondrial membrane, as in the late phase of infection the wild-type pVI is produced in massive amounts (Acheson, 2011). Importantly, Moyer et al. 2011 have shown that a single point mutation in the amphipathic helix, replacing the leucine at position 40 with a glutamine (L40Q), significantly impairs the protein's ability to insert into membranes (Figure 2). Additionally, a deletion mutant that lacks the complete amphipathic helix domain (55-239) should in theory be deficient in membrane disruption as well (Figure 2). Therefore, the L40Q and 55-239 mutant variants of pVI will play an important role as negative controls when investigating the protein's ability to associate with the mitochondrial membrane.

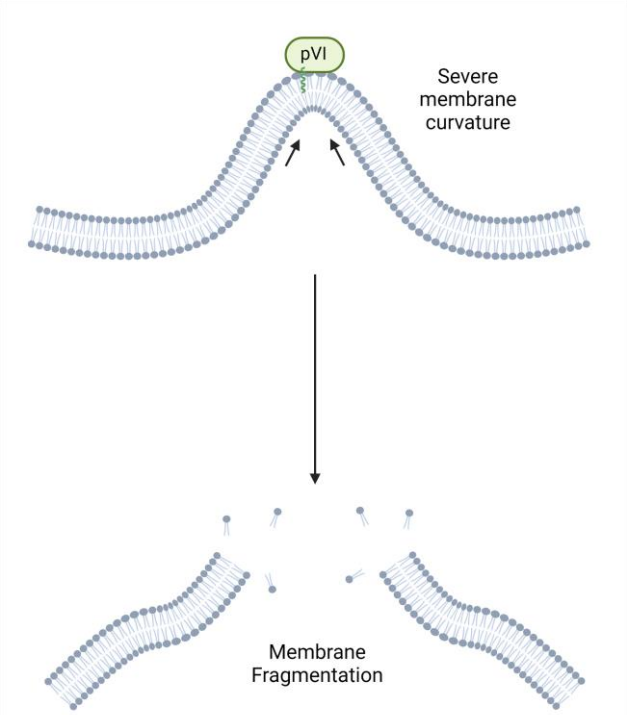

Figure 3. A simplistic visualization of the pVI mediated membrane fragmentation as proposed by Moyer et al. 2011. The amphipthatic helix of pVI anchors the protein into the membrane inducing a positive membrane curvature.

Aim

The aim of this thesis was to elucidate if and how the HAdV-C5 protein pVI contributes to the virus induced mtDNA release into the cytosol. Thus, this thesis seeks to study how the protein's localization to the mitochondria determines its disruptive nature with regards to mitochondrial membrane integrity, and subsequent mtDNA release. Furthermore, general effects on mitochondria elicited by pVI will be studied.

Materials and Methods

Cell Culture

HeLa-Kyoto, HeLa-Flp-In-T-Rex, HEK293T, U2OS and A549 cells were originally acquired from the American Type Culture Collection (ATCC). The cells were grown and maintained in Dulbecco´s modified Eagle medium (DMEM, Gibco™, GlutaMAX™) supplemented with 10 % fetal calf serum (FCS) and 2 % penicillin (10.000 units/mL)-streptomycin (10.000 mg/mL) (PEST) at 37 °C in a humidified atmosphere of 5 % CO_2. HeLa-Flp-In-T-Rex cells are derived from the classical HeLa-Kyoto cell line by integration of the doxycycline-regulatable repressor gene (T-Rex) into the host cell chromosome (Mun, 2019).

Virus Infection

For all infections, purified replication-competent HAdV-C5-pVII-Flag virus was used (Mun, 2019). Cells were infected at a multiplicity of infection (MOI) of 10-50 fluorescence-forming units (FFU) per cell in infection media (DMEM) supplemented with 2 % newborn calf serum (NCS) and 2 % PEST. The virus infected cells were incubated for 1 hour at 37 °C in 5 % CO_2. After incubation, the infection media was replaced with normal growth media (DMEM supplemented with 10 % FCS, 2 % PEST). Cells were harvested at 24 hours post infection unless otherwise stated.

Plasmids, siRNA, and codon-optimization

Plasmids expressing HAdV-C5 pVI wild-type (wt, also referred to as 1-250) and mutants (L40Q, 34-239, 55-239) were cloned into a pcDNA 3.1 vector expressing a C-terminal Haemagglutinin (HA) or N-terminal eGFP epitope tag, recognized with the anti-HA or anti-GFP antibody, respectively. As a control, the pcDNA 3.1 vector was used. The following fluorescently tagged plasmid constructs were used as markers for confocal microscopy: mApple-TOMM20-N-10 (Addgene plasmid #54955) and Rab5a-pmCherry-C1 (Addgene plasmid #27679). Due to limited expression and detection with anti-HA or anti-pVI primary antibodies via western blot analysis, the wild-type pVI (pVI(1-250)-HA) was codon-optimized at GenScript Biotech. The codon-optimized pVI (wt) plasmid was used as a template to generate target codon-optimized mutants either via deletion primer design or site directed mutagenesis (Quick change XL II, Agilent). All plasmid transfections were carried out using the jetPRIME® transfection reagent (Polyplus transfection®) according to the manufacturers protocol. To increase cell viability, transfection media was replaced with fresh growth media approximately 4 hours post transfection. To eliminate Bax, Bak and Tomm40 expression, following siRNAs (siGENOME SMART pool, Dharmacon) were used: human Bax (M-003308-03-0005), human Bak (M-003305-02-0005), human Tomm40 (M-012732-00-0005). SiRNAs were transfected using the jetPRIME® transfection reagent to a final concentration of 45 nM. As a control, a non-specific siRNA (Scrambled (“47 % GC”, 5´- AGGUAGUGUAAUCGCCUUG-3´, Eurofins) was used.

Subcellular Fractionation

Subcellular fractionation into cytosolic, mitochondrial, and nuclear compartments of cells was done using the Cell Fractionation Kit (Abcam, ab109719) according to the manufacturers protocol with some adjustments. Approximately, 5×10^6 cells were pelleted and re-suspended in 5 mL buffer A from the kit. The cells were counted and centrifuged at 300 × g for 5 minutes at 4 °C using a Megafuge 16R Thermo Scientific centrifuge. The resulting pellet was re-suspended in an equivalent volume of buffer A to reach a cell concentration of 6.6×10^6 cells/mL. From this pool of cells, 300 µl of suspended cells were aliquoted in 2 mL round-bottom Eppendorf tubes to be fractionated and 100 µl of suspended cells were aliquoted for

total DNA extraction used for qPCR normalization. The 300 µl of cells to be fractionated were mixed with an equal volume of buffer B (Cytosolic lysis buffer) followed by incubation at room temperature for 7 minutes on an end-over-end rotator. After incubation, the cells were centrifuged at 5000 × g for 1 minute at 4 °C and the supernatant was transferred to fresh tubes. This supernatant was then centrifuged twice at 1000 × g for 3 minutes at 4 °C and transferred to fresh tubes after each centrifugation step. Lastly the supernatant was centrifuged at 17.000 × g for 10 minutes at 4 °C to remove any remaining mitochondrial, nuclear, Golgi or ER contamination, producing pure cytosolic fractions. The resulting supernatant was transferred to fresh tubes and labelled as cytosolic fraction (C). The pellet containing the mitochondrial and nuclear fractions was resuspended in 300 µl buffer A and mixed with an equal volume of buffer C (mitochondrial lysis buffer) followed by incubation at room temperature for 10 minutes on an end-over-end rotator. After incubation, the cells were centrifuged at 5000 × g for 1 minute at 4 °C. The supernatant was transferred to fresh tubes and centrifuged at 10.000 × g for 1 minute at 4 °C. The resulting supernatant was then transferred to fresh tubes and labelled as mitochondrial fraction (M). The remaining pellet containing the nuclear fraction was lysed in 600 µl radioimmunoprecipitation (RIPA) buffer (25 mM Tris-HCL pH 7.5, 150 mM NaCl, 1 % NP40, 1 % Sodium deoxycholate and 0.1 % SDS) for 1 hour on ice. After 1 hour incubation the lysate was sonicated for 10 cycles (30 second on-off per cycle) and centrifuged at 17.000 × g for 10 minutes at 4 °C. The lysate was transferred into fresh tubes and labelled as nuclear fraction (N). The quality of the fractionation process was determined by the localization of tubulin or GAPDH for the cytosolic fraction (C), CoxIV for the mitochondrial fraction (M) and histone 3 for the nuclear fraction (N) by western blot analysis.

Isolation of total DNA and cytosolic mitochondrial DNA

For total DNA extraction, the 100 µl of suspended cells that were aliquoted for qPCR normalization in the subcellular fractionation process, were centrifuged at 6000 × g for 3 minutes at 4 °C. The pellets were then re-suspended in 500 µl 50 mM NaOH and incubated at 95 °C for 1 hour. After incubation, the NaOH was neutralized with 50 µl Tris-HCL pH 8.0. The total DNA extract was then centrifuged at 4000 rpm for 5 minutes at 4 °C and transferred into fresh 1.5 mL low DNA binding tubes. Alternatively, the cell pellets were lysed in 200 µl PBS and the total DNA was extracted using the QIAamp DNA Mini Kit (QIAGEN) according to the manufacturers protocol. 100 µl of total DNA was eluted in 1.5 mL low DNA binding tubes.

Cytosolic DNA extraction was done using the QIAquick Nucleotide Removal Kit (QIAGEN). Aliquots of 50 µl of the pure cytosolic fraction (C) produced from the subcellular fractionation were mixed with 250 µl of buffer PNI provided by the kit (1:5 volumes). The DNA was extracted by following the manufacturers protocol. 100 µl of cytosolic DNA was eluted in 1.5 mL low DNA binding tubes.

Quantitative PCR (qPCR) for detection of cytosolic mitochondrial DNA

qPCR reactions for the total and cytosolic DNA were prepared using the iTaq™ Universal SYBR® Green Super mix (Bio-Rad) according to the manufacturer's recommendations. The primers utilized for mtDNA detection are shown in Table 1. The DNA was amplified with the CFX384 Touch Real-Time PCR Detection System (Bio-Rad) using the following thermal cycling protocol: polymerase activation and DNA denaturation at 95 °C for 2 minutes, denaturation at 95 °C for 5 seconds and annealing/extension at 60 °C for 30 seconds for 40 cycles. qPCR results were analyzed with the CFX Maestro Software (Bio-Rad). The values of the cytosolic mtDNA data were normalized to the total mtDNA. Data is shown as the relative enrichment by taking non-treated samples as 1.

Table 1. Primers used for mitochondrial DNA detection

Target	Forward	Reverse	Source
NADH-ubiquinone oxidoreductase chain 1 (mt-ND 1)	5′-CCTAGCCGTTTACTCAATCCT-3′	5′-TGATGGCTAGGGTGACTTCAT-3´	Sigma
NADH-ubiquinone oxidoreductase chain 4 (mt-ND 4)	5´-TTGAAGTCCTTGAGAGAGGA-3´	5´-CCATCCTCCATATATCCAAA-3´	Sigma
Cytochrome B (mt-CytB)	5´-CCAATGATGGTAAAAGGGTA-3´	5´-GAGTCAACGGATTTGGTCGT-3´	Sigma
16S ribosomal RNA (mt-16S)	5′-CCTAGGGATAACAGCGCAAT -3′	5′-TAGAAGAGCGATGGTGAGAG 3′	Sigma

Western blot analysis

Cells were washed with ice-cold PBS (137 mM NaCl, 2.7 mM KCl, 10 mM Na_2HPO_4 and 1.8 mM KH_2PO_4) and afterwards lysed in radioimmunoprecipitation (RIPA) buffer (25 mM Tris-HCL pH 7.5, 150 mM NaCl, 1 % NP40, 1 % Sodium deoxycholate and 0.1 % SDS) on ice and stored -20 °C. The lysates of harvested cells or nuclear fractions from fractionation experiments were sonicated for 10 cycles (30 seconds on-off per cycle) and centrifuged at 17.000 × g for 10 minutes at 4 °C. Each lysate was mixed (1:4) with 5 × SDS loading dye (Abcam) followed by heating at 95°C for 5 minutes. The samples were equally loaded and separated by sodium dodecyl sulphate polyacrylamide gel electrophoresis (SDS-PAGE) using homemade 5 % stacking and 12.5 % or 13.5 % separation gels (protocol available at http://www.changbioscience.com/calculator/sdspage.html). SDS-PAGE was run in 1 × SDS-PAGE running buffer (25 mM Tris, 192 mM Glycine, 0.1 % SDS pH 8.3 for 10 ×). Separated proteins were transferred to a nitrocellulose membrane (Merck Millipore) using the Towbin transfer buffer (25 mM Tris, 192 mM Glycine) supplemented with 10 % methanol. After protein transfer the membranes were briefly washed with 1× TBST (20 mM Tris, 1500 mM, NaCl pH 7.6 and 0.1 % Tween 20) and blocked with blocking buffer (Intercept, LI-COR) for 20-40 minutes followed by incubation with primary antibodies (Table 2) at 4 °C overnight. After incubation, the membranes were washed 4 × 5 minutes with TBST and probed with fluorescence-labelled secondary antibodies (IRDye®, LI-COR). Ensuing secondary antibody incubation, the membranes were washed again 4 × 5 minutes with TBST and the protein bands were visualized by the Odyssey CLX imaging system (LI-COR). Page Ruler™ plus pre-stained protein ladder (Thermo Scientific) was used as a size standard for protein size determination.

Immunofluorescence assay

Hela-Kyoto cells were seeded onto 10 mm borosilicate coverslips (VWR™) in a 24-well plate format (Sarstedt) and grown at 37 °C, 5 % CO_2 overnight in DMEM supplemented with 10 % FCS and 2 % PEST. The cells were transfected with the previously mentioned plasmid pVI constructs (Plasmids section) and then grown for another 24 hours. The cells were washed twice with 1 mL of PBS followed by placement of the coverslips onto a parafilm. Ensuing, the cells were fixed with 4 % PFA/PBS for 15 minutes at room temperature and then permeabilized with 0.1 % Triton-X-100 (Merck)/PBS for another 15 minutes at room temperature. Upon removal of the permeabilization solution the cells were washed 3 times with 0.1 % PBST and blocked with PBST/Glycine/BSA for 1 hour at room temperature. The primary antibodies (Table 2) were diluted 1:1000 in PBST/BSA and added onto the coverslips followed by incubation ON at 4 °C in a humidified container. After incubation, the cells were washed 3 times with PBST/BSA and probed with secondary antibodies diluted 1:2000 (Alexa Fluor, 594 chicken anti-rabbit IgG 2 mg/mL, Invitrogen, A21442 and Alexa Fluor 488 goat anti-mouse IgG 2 mg/mL, Invitrogen, A11001) for 30 minutes at room temperature. After one wash with PBST/BSA the cells were incubated with 300 nM DAPI for 5 minutes at room temperature. Finally, the coverslips were washed 3 times with PBST/BSA and mounted onto glass-slides with a drop of ProLong™ (Thermo Scientific) mounting media. The cells were analyzed with the NIKON 90i microscope at 60× magnification.

Table 2. Antibodies

Target	Concentration	Host	Source	Identifier
Anti-pVI (9F10)	1 mg/mL	Mouse, monoclonal	Merck Millipore	Cat# MABF2196-100UG
Anti-HA.11	1 mg/mL	Mouse, monoclonal	BioLegend	Cat# MMS-101P
Anit-E1B-19k		Rabbit	Lomonosova et al., 2005	
Anti-Histone 3	0.9 mg/mL	Rabbit, polyclonal	Abcam	Cat# ab1791
Anti-GAPDH (FL-335)	200 µg/mL	Rabbit, polyclonal	SantaCruz	Cat# sc-25778
Anti-Tubulin (6A204)	200 µg/mL	Mouse, monoclonal	SantaCruz	Cat# sc-69969
Anti-Actin (I-19)	100 µg/mL	Goat, polyclonal	SantaCruz	Cat# sc-1616
Anti-CoxIV	353 µg/mL	Rabbit, polyclonal	Proteintech	Cat# 11242-1-AP
Anti-Tomm40	333 µg/mL	Rabbit, polyclonal	Proteintech	Cat# 18409-1-AP
Anti-Bax (2D2)	200 µg/mL	Mouse, monoclonal	SantaCruz	Cat# sc-20076
Anti-Bak (D4E4)	100 µg/mL	Rabbit, monoclonal	Cell Signaling Technology	Cat# 12105

Subcellular localization of fluorescently tagged proteins using spinning disc confocal microscopy (Collaboration)

HeLa-Kyoto cells were seeded onto 25 mm round coverslips (Mentzer-Glaser) in a 6-well plate format (Sarstedt) and grown at 37 °C, 5 % CO_2 overnight in DMEM supplemented with 10 % FCS and 2 % PEST. The cells were co-transfected with the GFP tagged pVI constructs and mApple-Tomm20 or mCherry-Rab5 protein expressing plasmids for 24 hours.

The subcellular localization of fluorescently tagged proteins was determined using a spinning disc confocal microscope. The setup is built around a Nikon Ti2 microscope equipped with a Yokogawa CSU-10 spinning disc confocal unit. Light for excitation of GFP and mCherry was delivered by 491-nm and 561-nm DPSS lasers, respectively (Cobolt, Solna, Sweden). The excitation light was homogenized by a rotating light-shaping diffusor and focused into the confocal unit. Fluorescence was collected through a 100X 1.49 plan-Apo objective (Nikon) and emission detected with a back-illuminated EM-CCD camera (Andor iXon DU-888) using 530/50-nm and 590-LP filters mounted in a filter wheel (Lambda 10-3, Sutter Instruments). Light exposure between image captures was prevented using electronic shutters (Sutter Instruments). The microscope setup was controlled by MetaFluor software (Molecular Devices corp.). Prior to experiments, cells grown on 25 mm round coverslips were washed and placed in an experimental buffer containing 125 mM NaCl, 5 mM KCl, 1.2 mM $MgCl_2$, 1.3 mM $CaCl_2$, 25 mM Hepes with pH adjusted to 7.40. The coverslips were used as exchangeable bottoms in a modified Sykes-Moore chamber that was placed in a custom-built holder on the stage of the microscope and maintained at 37°C throughout the experiment[1].

Mitochondrial membrane potential measurements using TMRM and epifluorescence microscopy (Collaboration)

HeLa-Kyoto cells were seeded onto 25 mm borosilicate coverslips (Mentzer-Glaser) in a 6-well plate format (Sarstedt) and grown at 37 °C, 5 % CO_2 overnight in DMEM supplemented with 10 % FCS and 2 % PEST. The cells were transfected with the plasmids expressing the pVI (wt)-HA and pVI (L40Q)-HA proteins for 24 hours.

The mitochondrial membrane potential ($\Delta\Psi_m$) was monitored by the lipophilic cationic dye tetramethylrhodamine methyl (TMRM, Image-iT™ ThermoFisher) via fluorescence time-lapse imaging using an inverted microscope (Eclipse TE2000U; Nikon, Kanagawa, Japan). The epifluorescence microscope was equipped with a high-power LED light source (Omicron LedHUB; Photonlines Ltd, Newcatle, UK) which provided excitation light at 550 nm (572 nm with 15 nm half-bandwidth) through a 5-mm diameter liquid light guide. Emission light was selected with a 593LP filter and the fluorescence signal was detected by an EM-CCD camera (Evolve EMCCD; Photometrics, Arizona, USA). The MetaFluor software (Molecular Devices corp.) allowed to control the microscope setup and to acquire images every 5 seconds. Prior to imaging, the cells were loaded with TMRM (10 nM) during a 30 min incubation at 37 °C in a buffer containing 125 mM NaCl, 5 mM KCl, 1.3 mM $CaCl_2$, 1.2 mM $MgCl_2$, and 25 mM HEPES with pH adjusted to 7.40 with NaOH. The coverslips were placed in the bottom of an open Sykes-More chamber. On the top of the coverslip, a thin 25-mm diameter stainless steel plate with a 4-mm wide and 7-mm long opening pressed the 1-mm thick silicon rubber gasket with identical dimensions and central opening to the coverslip. The temperature of the chamber holder and the CFI S Fluor 40 x 1.3 numerical aperture oil immersion objective (Nikon) were kept at 37°C during the experiment using custom-built thermostats. Fixed on the stainless-steel plate, inlet and outlet cannulas maintained a laminar superfusion at a rate of 2.0 mL/min with the imaging buffer containing 10 nM TMRM or 10 µM FCCP (Sigma) throughout the experiment[1].

[1] Expertise kindly provided by Dr. Olof Idevall and Styliani Panagiotou (Department for Medical Cell Biology, Uppsala University)

Results

HAdV-C5 infection induces release of mtDNA into the cytosol.

It was previously shown that infection with HAdV-C5 leads to an increased abundance of mtDNA in the cytosol of HeLa cells (Mun, 2019). However, the main problem with this study was the reproducibility of the results. To gain a better reproducibility for these experiments, the protocol for the isolation and detection of released mtDNA was optimized (see Materials and Methods section). Following this established protocol, HeLa-Flp-In-T-Rex cells were infected with replication competent HAdV-C5-pVII-Flag virus with a multiplicity of infection (MOI) of 10 FFU. At 24 hours post infection (hpi), infected and non-infected (i-. e., mock) cells were fractionated into cytosolic (C), mitochondrial (M), and nuclear (N) fractions. The resulting cytosolic fractions were subsequently analyzed for the presence of mtDNA with quantitative PCR (qPCR) utilizing primers that target different regions of the mitochondrial genome (Table 1). Notably, virus infection induced an approximately 5-fold increase in cytosolic mtDNA as compared to mock-infected cells 24 hpi (Figure 4A). As proof of successful infection, subcellular fractions were tested for the expression of the viral late protein pVI, which localized to all three fractions, including the mitochondrial fraction (Figure 4B). Interestingly, the lower band speculated to depict the mature form of pVI (34-239) had a more prominent mitochondrial accumulation than the wild-type protein (Figure 4B).

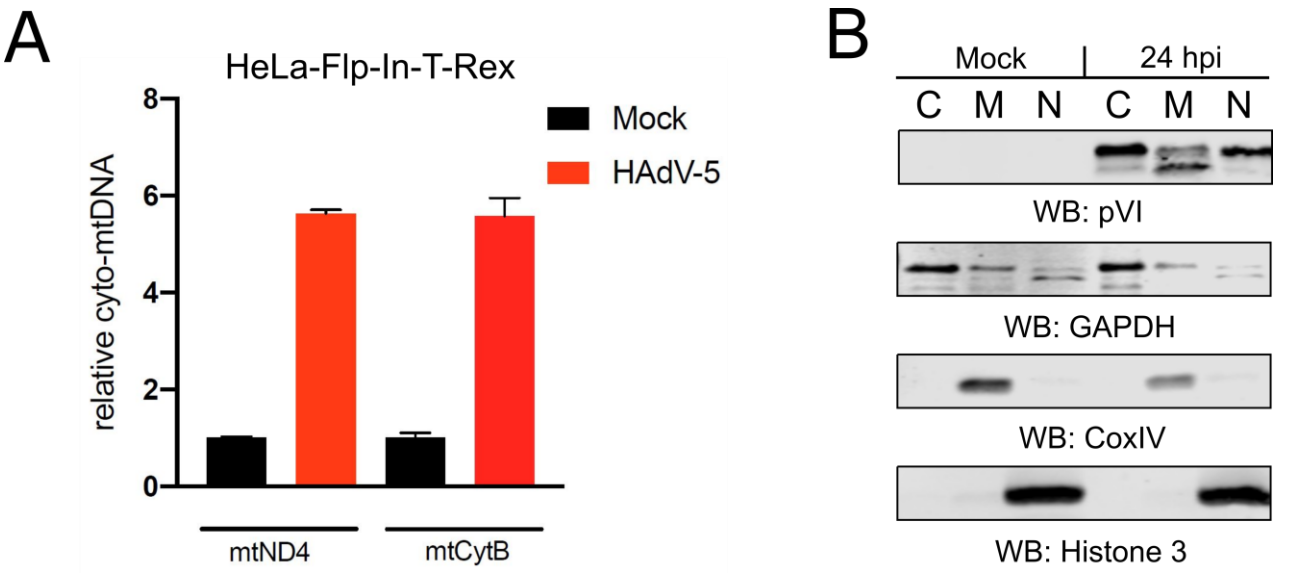

Figure 4. HAdV-C5 infection induces release of mtDNA into the cytosol. A HeLa-Flp-In-T-Rex cells were infected with HAdV-C5 virus and fractionated 24 hours post infection (hpi). Relative cytosolic mtDNA (Fold) was detected with qPCR utilizing the mt-ND4 and mt-CytB gene primers. The obtained cytosolic mtDNA values were normalized to the total mtDNA values. Data shown as relative enrichment of cyto-mtDNA by taking non-infected (mock) cells as 1. **B** Western blot analysis for the subcellular fractionation of the HAdV-C5 infected HeLa-Flp-In-T-Rex cells. The quality of the cytosolic (C), mitochondrial (M) and nuclear (N) fractions was analyzed using antibodies targeting GAPDH, CoxIV and histone 3, respectively. Protein pVI was detected with the anti-pVI antibody. The cytosolic fractions were used for mtDNA detection.

To further investigate the temporal pattern of mtDNA release, HeLa-Flp-In-T-Rex cells were infected for 4, 10 and 27 hours. Analysis of the cytosolic fractions revealed an expected increase of cyto-mtDNA after 27 hpi (Figure 5A), correlating with protein pVI accumulation during the late phase of infection (Figure 5B). Consistent with the previous experiment (Figure 4), the pVI protein showed distinctly lower bands (i.e., faster migrating proteins) accumulating mainly in the mitochondrial fraction on a 13.5% polyacrylamide gel (Figure 5B). This implies that the pVI has a mitochondrial association. The viral early protein E1B-19k, known to associate with the Bax and Bak proteins, became visible 10 hpi in the

mitochondrial fraction (Figure 5B). Surprisingly, an increase in cytosolic mtDNA was also apparent after 4 and 10 hpi (Figure 5B), suggesting that either viral early proteins or mature forms of infecting virus capsid proteins may induce mitochondrial stress during the early phase of infection.

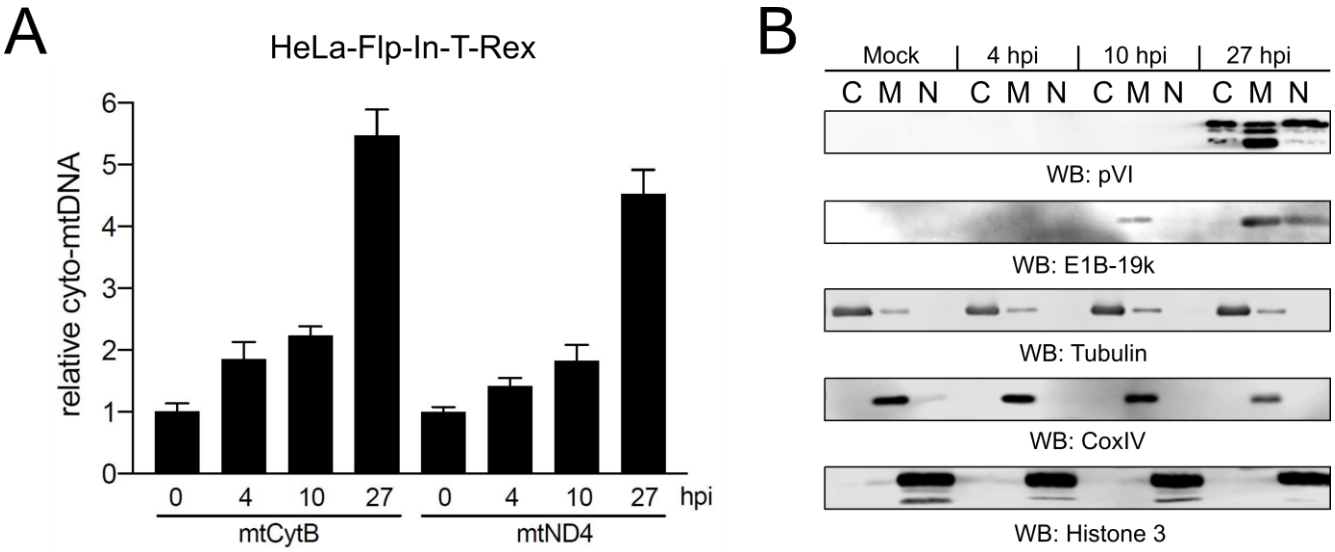

Figure 5. HAdV-C5 induced mtDNA release correlates to pVI production. A HeLa-Flp-In-T-Rex cells were infected with HAdV-C5 and fractionated at the indicated hours post infection (hpi). Relative cytosolic mtDNA (Fold) for each time point was detected with qPCR utilizing the mt-CytB and mt-ND4 gene primers. Results are shown after normalization of the cytosolic mtDNA to the total mtDNA. Timepoint 0 depicts mock infected cells. **B** Western blot analysis for the subcellular fractionation of infected HeLa-Flp-In-T-Rex cells. The purity of the cytosolic (C), mitochondrial (M) and nuclear (N) fractions was analyzed using antibodies targeting tubulin, CoxIV and histone 3, respectively. Protein pVI was detected with the anti-pVI antibody and E1B-19k with the anti-E1B-19k antibody. The cytosolic (C) fractions were used for cyto-mtDNA detection.

To determine whether the HAdV-C5 induced mtDNA release was not HeLa cell line specific, U2OS cells were infected with a MOI of 10 FUU and 50 FFU. The U2OS cell line is an osteosarcoma cell line and used as one of the cell models to study HAdV infections. Notably, HAdV-C5 late (capsid) protein production is delayed in U2OS as this cell line grows slower than HeLa cells (Mun, 2019). Therefore, the cells were fractionated 42 hpi followed by qPCR analysis of mtDNA in the cytosolic fractions. As shown in Figure 6A, HAdV-C5 infection also caused cyto-mtDNA accumulation in U2OS cells. The abundance of the cyto-mtDNA in MOI 10 and MOI 50 infected cells was similar for the mtND4 and mtND1 amplicons, suggesting that the observed mtDNA release is time-dependent rather than virus particle number (MOI) dependent (Figures 4 through 6). Biochemical analysis of the fractionation showed that in U2OS cells, pVI accumulated in the cytosolic and mitochondrial fractions (Figure 6B). This accumulation was stronger in MOI 50 infected cells compared to MOI 10. Interestingly, the pVI band in the mitochondrial fraction was distinctly lower than the band in the cytosolic fraction, which probably depicted the full-length protein (Figure 6B). This observation is in line with the lowest pVI band detected in the mitochondrial fraction of HeLa cells. Surprisingly, pVI did not localize to the nuclear fraction in U2OS cells, and the full-length protein was not detected in the mitochondrial fraction as seen in HeLa cells (Figure 6B and figure 5B). This suggests that the protein behaved differently in U2OS cells than in HeLa, but still localized to the mitochondrial fraction and induced mtDNA release into the cytosol (Figure 6A).

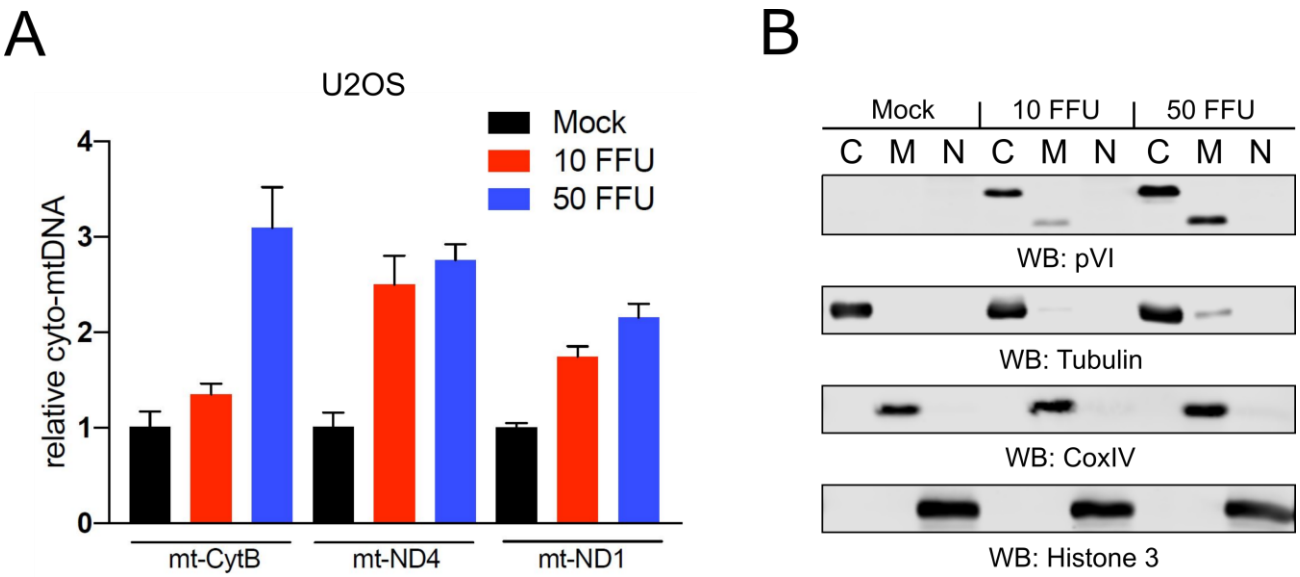

Figure 6. HAdV-C5 infection induces release of mtDNA in U2OS cells. A U2OS cells were infected with HAdV-C5 with a MOI of 10 FFU and 50 FFU. The cells were fractionated 42 hpi. Relative cytosolic mtDNA (fold) was detected with qPCR utilizing the mt-CytB, mt-ND4 and mt-ND1 gene primers. The obtained cytosolic mtDNA values were normalized to the total mtDNA values. **B** Western blot analysis for the subcellular fractionation of the HAdV-C5 infected U2OS cells. The quality of the cytosolic (C), mitochondrial (M) and nuclear (N) fractions was analyzed using antibodies targeting tubulin, CoxIV and histone 3, respectively. Protein pVI was detected with the anti-pVI antibody. The cytosolic fractions were used for mtDNA detection.

The HAdV-C5 pVI protein's amphipathic helix is involved in cyto-mtDNA release.

The previously mentioned data indicated that the pVI protein strongly accumulated in the mitochondrial fraction during virus infection (Figures 4, 5 and 6). To elucidate involvement of pVI in the virus induced mtDNA release, plasmids expressing the pVI-HA protein were generated. Notably, anti-pVI and anti-HA antibodies had limited detection of the pVI protein expressed from the plasmid (Figure 6A). Since several of HAdV-C5 proteins show increased protein expression after their cDNA has been codon-optimized (Inturi et al., 2013), the pVI (wt) cDNA was also codon optimized to increase protein production. As shown in Figure 7A, pVI codon optimization clearly increased expression of the pVI-HA protein.

The N-terminal amphipathic helix located within pVI amino acids 36-55 has been shown to exhibit membrane lytic activity (Wiethoff and Nemerow, 2015). To investigate whether this activity of pVI could be linked to mitochondrial membrane disruption and mtDNA release, the codon optimized HA-tagged pVI (wt), pVI (34-239) and pVI (55-239) proteins (Figure 2) were transiently overexpressed in HeLa-Flp-In-T-Rex cells. Subsequently, the cells were fractionated 22 hours post transfection. Analysis of the cytosolic fractions revealed that both the wild type (1-250) and mature (34-239) pVI induced mtDNA release into the cytosol (Figure 7B). The mutant lacking the amphipathic helix (55-239) induced notably lower cyto-mtDNA accumulation (Figure 7B). Biochemical analysis of the fractionation depicted a weak detection of the pVI (1-250) and pVI (34-239) proteins in mitochondrial and nuclear fractions, whereas the pVI (55-239) protein strongly located to the cytosolic fraction when detected with the anti-HA antibody (Figure 7C). Surprisingly, when detected with the anti-pVI antibody, all three proteins (1-250, 34-239 and 55-239) were detected as truncated proteins strictly located in the mitochondrial fraction (Figure 7C). The protein levels of the truncated pVI versions correlated to the relative mtDNA released, as the less prominent pVI (55-239) induced the lowest levels of cyto-mtDNA (Figure 7B). This result implies that the amphipathic helix is important for the proteins interaction with the mitochondria but may not solely be responsible for

mtDNA release. Additionally, the truncated versions of pVI shown in the overexpression experiment (Figure 7B) coincide with the shorter bands observed in the virus infection (Figures 4B, 5B and 6B).

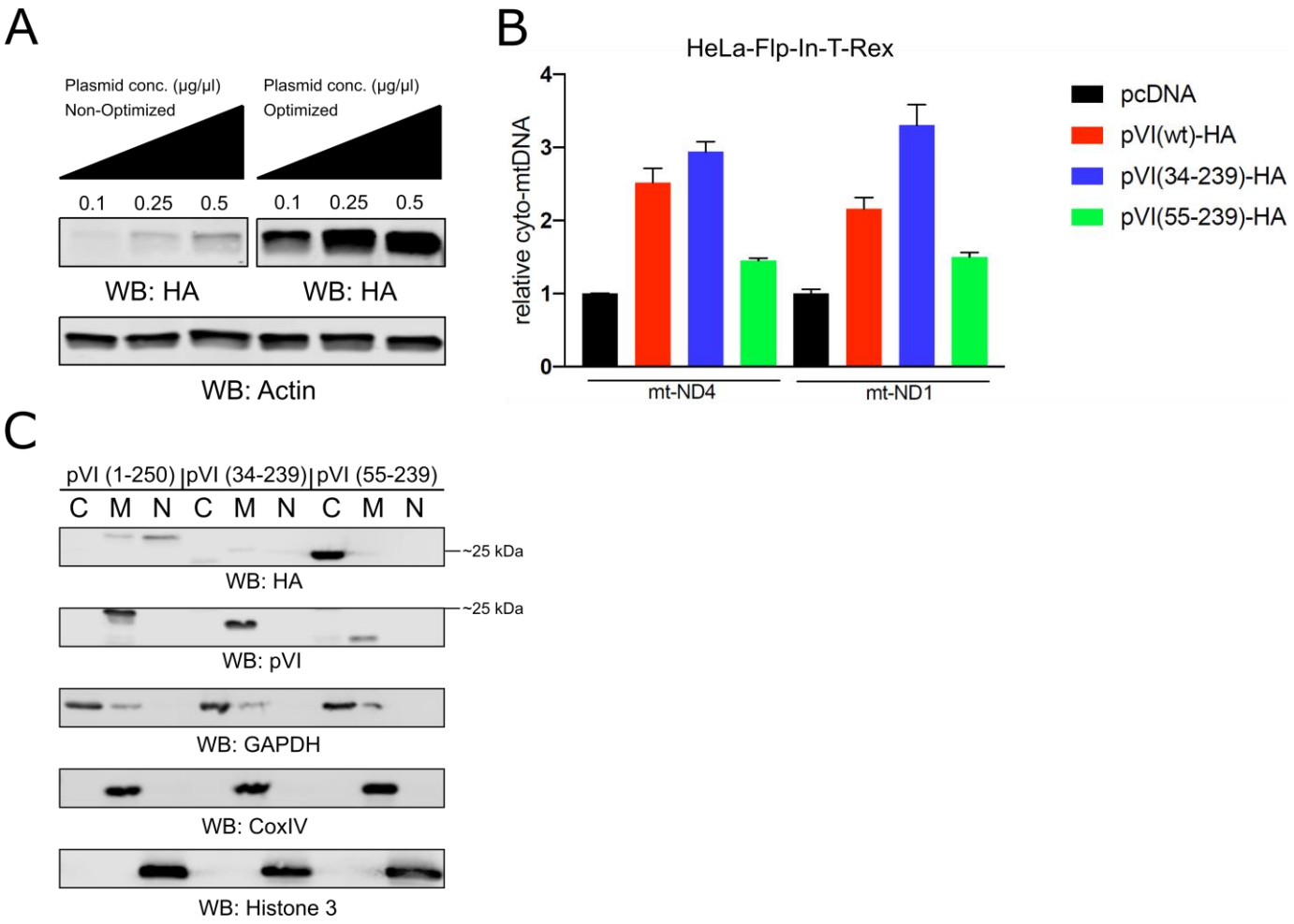

Figure 7. HAdV-C5 pVI protein induces mtDNA release. A HEK293T cells were transfected with plasmids expressing the non-codon optimized and codon optimized pVI (wt)-HA proteins for 24 hours. Plasmids were transfected in increasing concentrations of 0.1, 0.25 and 0.5 µg/µl. The pVI protein was detected with the anti-HA antibody. Detection of actin was used as the loading control. **B** HeLa-Flp-In-T-Rex cells were transfected with plasmids expressing the codon optimized pVI (1-250)-HA, pVI (34-239)-HA and pVI (55-239)-HA proteins. The cells were fractionated 22 hours post transfection. The cytosolic mtDNA was analyzed with qPCR using the mt-ND4 and mt-ND-1 gene primers. Cells transfected with pcDNA for 22 hours were used as control. Cyto-mtDNA values were normalized to the total mtDNA values. **C** Western blot analysis for the subcellular fractionation of the transfected HeLa-Flp-In-T-Rex with the indicated pVI versions. The quality of the cytosolic (C), mitochondrial (M) and nuclear (N) fractions was analyzed using antibodies targeting GAPDH, CoxIV and histone 3, respectively. Protein pVI was detected with the anti-HA and anti-pVI antibodies. The cytosolic fractions were used for mtDNA detection.

Moyer et al. 2011 have shown that a point mutation in the amphipathic helix, changing the leucine (L) at amino acid position 40 to a glutamine (Q) (L40Q), significantly reduces the membrane association for pVI. To investigate whether the L40Q point mutation reduces the pVI induced mtDNA release, pVI (wt)-HA and pVI (L40Q)-HA proteins were transiently overexpressed in HeLa-Flp-In-T-Rex and A549 cells. The cells were fractionated approximately 22 hours post transfection. Strikingly, in HeLa cells the pVI (wt) protein induced an 8 up to 9-fold increase in cyto-mtDNA when compared to the control (pcDNA) (Figure 8A). Further, the L40Q mutant induced a drastically lower accumulation of cyto-mtDNA compared to the

wild-type protein, indicating the importance of the functional amphipathic helix (Figure 8A). A similar cyto-mtDNA pattern was observed in A549 cells that exhibit a lower transfection efficiency than HeLa cells (Figure 8C). In line with the data from HeLa cells, in A549 cells the pVI (L40Q) was less efficient in releasing mtDNA compared to the wild-type protein (Figure 8C). Biochemical analysis of the fractionation and detection with the anti-pVI antibody revealed that both the wild-type and L40Q mutant proteins appeared as truncated versions in the mitochondrial fraction of both HeLa and A549 (Figure 8B and 8D). Importantly, both proteins were equally expressed, indicating that the mtDNA release in pVI (L40Q) expressing cells was not due to differences in protein expression (Figure 8B and 8D). Taken together, these results show that pVI can induce mtDNA release and that the N-terminal amphipathic helix plays a major role in this function.

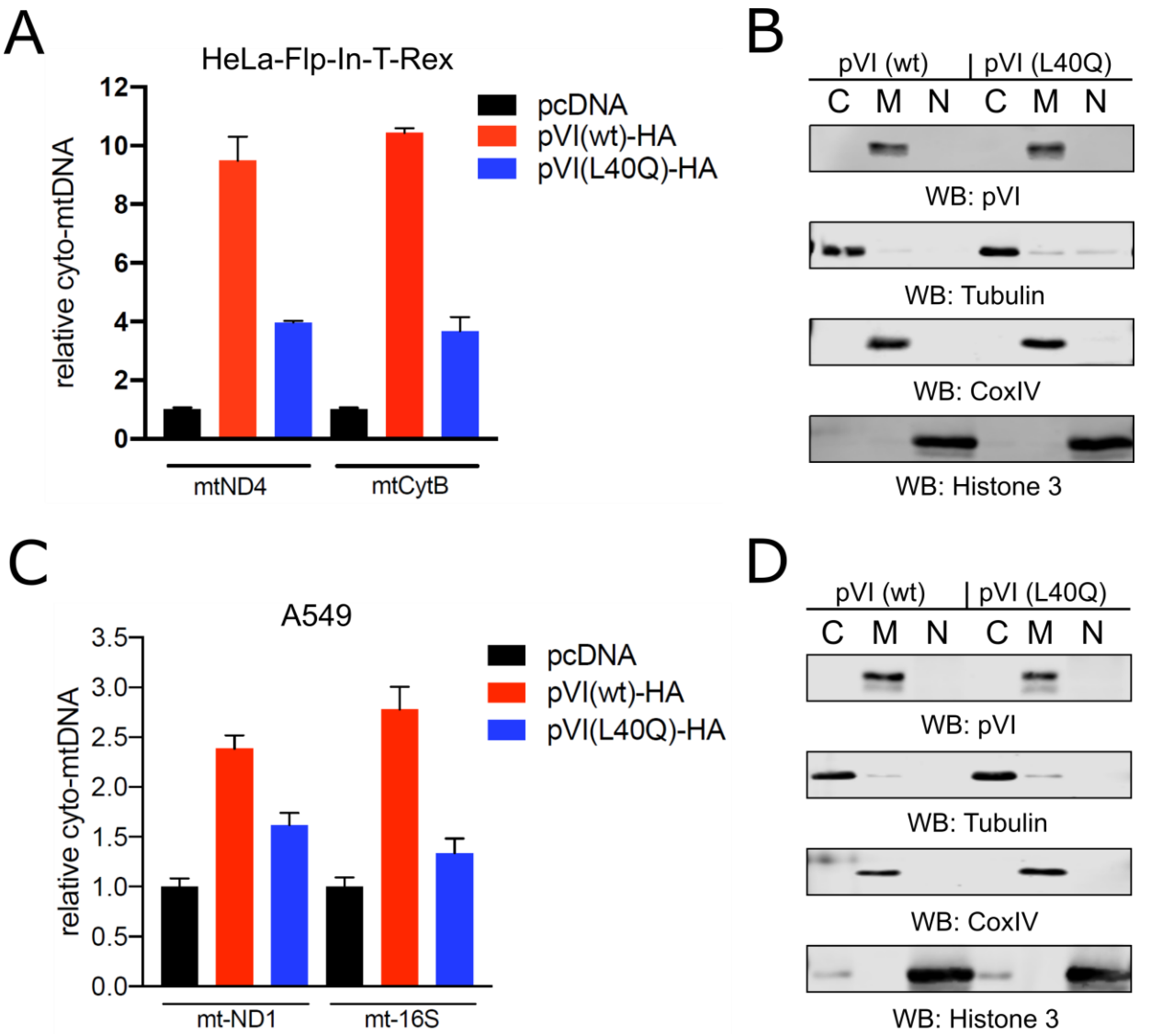

Figure 8. The pVI (L40Q) mutant is limited in cytosolic mtDNA release. A HeLa-Flp-In-T-Rex and **C** A549 cells were transfected with plasmids expressing the codon optimized pVI (wt)-HA and pVI (L40Q)-HA proteins. The cells were fractionated 22 hours post transfection. The cyto-mtDNA was detected with qPCR using the mt-ND4, mt-CytB, mt-ND1 and mt-16S primers. Transfection of pcDNA was used as control. Cyto-mtDNA values were normalized to the total mtDNA values. **B/D** Western blot analysis for the subcellular fractionation of the transfected HeLa **B** and A549 **D** cells expressing the indicated pVI proteins. Fractionation quality of the cytosolic (C), mitochondrial (M) and nuclear (N) fractions was assessed with antibodies targeting tubulin, CoxIV and histone 3, respectively. Protein pVI was detected with the anti-pVI antibody. The cytosolic fractions of the respective cell lines were used for mtDNA detection

The HAdV-C5 E1B-19k protein interferes with the pVI-mediated mtDNA release.
Previous studies have shown that the HAdV-C5 E1B-19k protein localizes to the mitochondria to sequester the pro-apoptotic Bax and Bak proteins, thereby preventing unwanted apoptosis in HAdV-infected cells (Han et al., 1996). Additionally, the Bax and Bak protein mediated MOMP can induce mtDNA efflux into the cytosol (McArthur et al., 2018). Consistent with these studies, E1B-19k appeared 10 hpi in the mitochondrial fraction of HAdV-C5 infected HeLa cells (Figure 5B). Thus, E1B-19k as well as Bax and Bak could potentially interfere with the pVI-mediated mtDNA release into the cytosol. To test this hypothesis, plasmids expressing the E1B-19k-HA and pVI-HA proteins were co-transfected into HeLa-Flp-In-T-Rex cells followed by subcellular fractionation 22 hours post-transfection. As expected, pVI expression induced cyto-mtDNA accumulation (Figure 9A). Transfection of the E1B-19k protein led to a minor decrease in cytosolic mtDNA compared to the control sample (pcDNA) (Figure 9A). Interestingly, overexpression of E1B-19k protein encoding plasmid together with pVI blocked the pVI-induced cyto-mtDNA accumulation (Figure 9A). This finding suggests a possible connection of the Bax and Bak proteins with the pVI mediated-mtDNA release in the absence of the E1B-19k protein. The biochemical fractionation showed that both pVI and E1B-19k are prominently present in the mitochondrial fraction (Figure 9B). Interestingly, co-transfection of E1B-19k with pVI lowered the E1B-19k protein accumulation in the mitochondria (Figure 9B). Collectively this data shows, for the first time, that the E1B-19k protein interferes with the pVI-mediated mtDNA release.

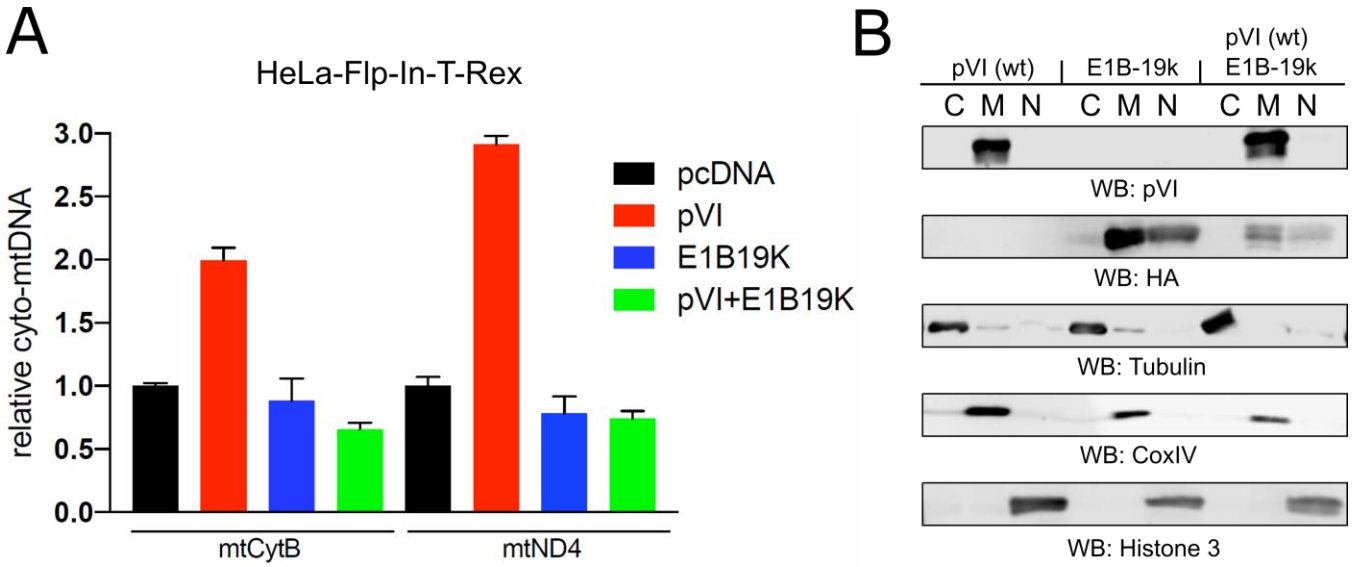

Figure 9. HAdV-C5 E1B-19k protein blocks pVI mediated mtDNA release. A HeLa-Flp-In-T-Rex cells were co-transfected with plasmids expressing the pVI (wt)-HA and E1B-19k-HA proteins. 22 hours post transfection the cells were fractionated. The cyto-mtDNA abundance was analyzed with the mt-CytB and mt-ND4 gene primers using qPCR. Cells transfected with pcDNA were used as control. Cytosolic mtDNA values were normalized to the total mtDNA values. **B** Western blot analysis for the subcellular fractionation of the transfected HeLa-Flp-In-T-Rex. The quality of the cytosolic (C), mitochondrial (M) and nuclear (N) fractions was analyzed using antibodies targeting tubulin, CoxIV and histone 3, respectively. Protein pVI and E1B-19k were detected with the pVI and anti-HA antibodies, respectively. The cytosolic fractions were used for cyto-mtDNA detection.

Elimination of the Bax/Bak and Tomm40 proteins affects pVI-mediated mtDNA release and pVI protein processing.
The inhibiting function of E1B-19k in the pVI-induced mtDNA release suggested an involvement of the Bax and Bak proteins in this process. To study this connection, HeLa-Flp-In-T-Rex cells were co-transfected with siRNAs targeting the endogenous Bax and Bak mRNAs for 48 hours. Subsequently, the pVI (wt)-HA protein was transiently overexpressed in knockdown and control cells. The cells were

fractionated approximately 22 hours post transfection. Interestingly, analysis of the cytosolic fractions indicated a clear decrease in the pVI protein's ability to induce mtDNA release when expressed in Bax and Bak knockdown cells (Figure 10A). This effect was more evident when analyzing the mtND1 amplicon. Biochemical analysis indicated a notable reduction of the Bax and Bak proteins. (Figure 10B). Together, this data suggests that the Bax and Bak proteins are involved in the pVI-mediated mtDNA release into the cytosol.

Analysis of mitochondrial fractions from previous experiments implicated that the pVI-HA protein (26 kDa) is processed into smaller versions (Figure 7C). The anti-pVI antibody detected full length and truncated versions of the protein approximately 3-5 kDa smaller, whereas the anti-HA antibody only detected the full-length protein. Proteins transported into the mitochondria pass through the translocases of the outer and inner mitochondrial membrane complexes, TOMM and TIMM respectively (Cooper, 2000). To investigate whether pVI enters mitochondria and is subsequently processed into shorter forms, similar to endogenous mitochondria targeting proteins, HeLa-Flp-In-T-Rex cells were transfected with siRNAs targeting the translocase of the outer mitochondrial membrane (Tomm40) mRNA for 48 hours. Knockdown of this essential protein channel reduces the transport of proteins through the outer mitochondrial membrane. After siRNA treatment, knockdown and control cells were transfected with the pVI (wt)-HA expressing plasmid for 22 hours. Subcellular fractionation, followed by analysis of cytosolic mtDNA showed that in both control and Tomm40 knockdown cells pVI stimulated the release of mtDNA (Figure 10A). Interestingly, visualization of the truncated versions of the pVI protein revealed that in the Tomm40 knockdown cells the protein is less accumulated and proteolytically processed (Figure 10B).

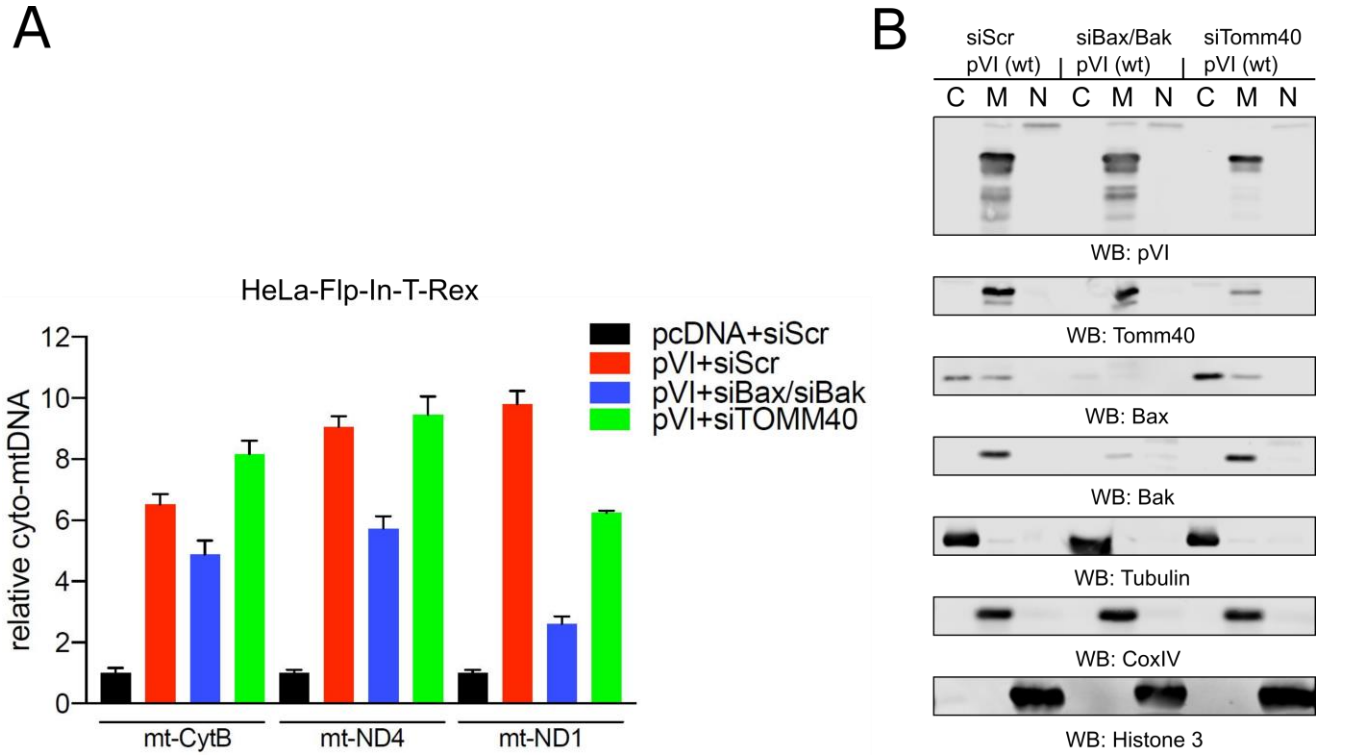

Figure 10. Knockdown of Bax/Bak and Tomm40 reduces pVI mediated mtDNA release and protein truncation, respectively. A HeLa-Flp-In-T-Rex cells were transfected with siRNAs targeting Bax and Bak as well as Tomm40 for 48 hours. Ensuing the cells were transfected with the pVI (wt)-HA protein expressing plasmid. Transfection of siScr and pcDNA was used as control. 22 post transfection the cells were fractionated. The levels of cyto-mtDNA were analysed with qPCR utilizing primers targeting the mt-CytB, mt-ND4 and mt-ND1 genes. Cytosolic mtDNA values were normalized to the total mtDNA values. **B** Western blot analysis of the knockdown efficiency and subcellular fraction of the transfected HeLa cells. The quality of the cytosolic (C), mitochondrial (M) and nuclear (N) fractions was analyzed using antibodies targeting tubulin, CoxIV and histone 3, respectively. Bax, Bak and Tomm40 were detected with antibodies targeting the respective protein. Protein pVI was detected with the anti-pVI antibody. The cytosolic fractions were used for mtDNA detection.

The HAdV-C5 pVI protein co-localizes with mitochondria.
In the biochemical subcellular fractionation experiments, pVI consistently localized to the mitochondrial fraction. This fraction however can still contain other cellular compartments, such as the endoplasmatic reticulum (ER). To visualize whether pVI colocalizes with mitochondria in single cells, HeLa-Kyoto cells were transiently transfected with plasmids expressing the pVI (wt) and pVI (wt)-HA proteins. The transfected cells were subsequently fixed and stained with the anti-pVI and anti-CoxIV antibodies, where CoxIV acted as the mitochondrial marker. In line with the biochemical fractionation experiments, immunofluorescence analysis revealed a clear co-localization of the pVI and CoxIV proteins, where the latter is located on the inner mitochondrial membrane (Figure 11). Importantly, the pVI-HA protein used in the biochemical fractionation experiments exhibited a nearly identical localization pattern with CoxIV as the un-tagged pVI (Figure 11).

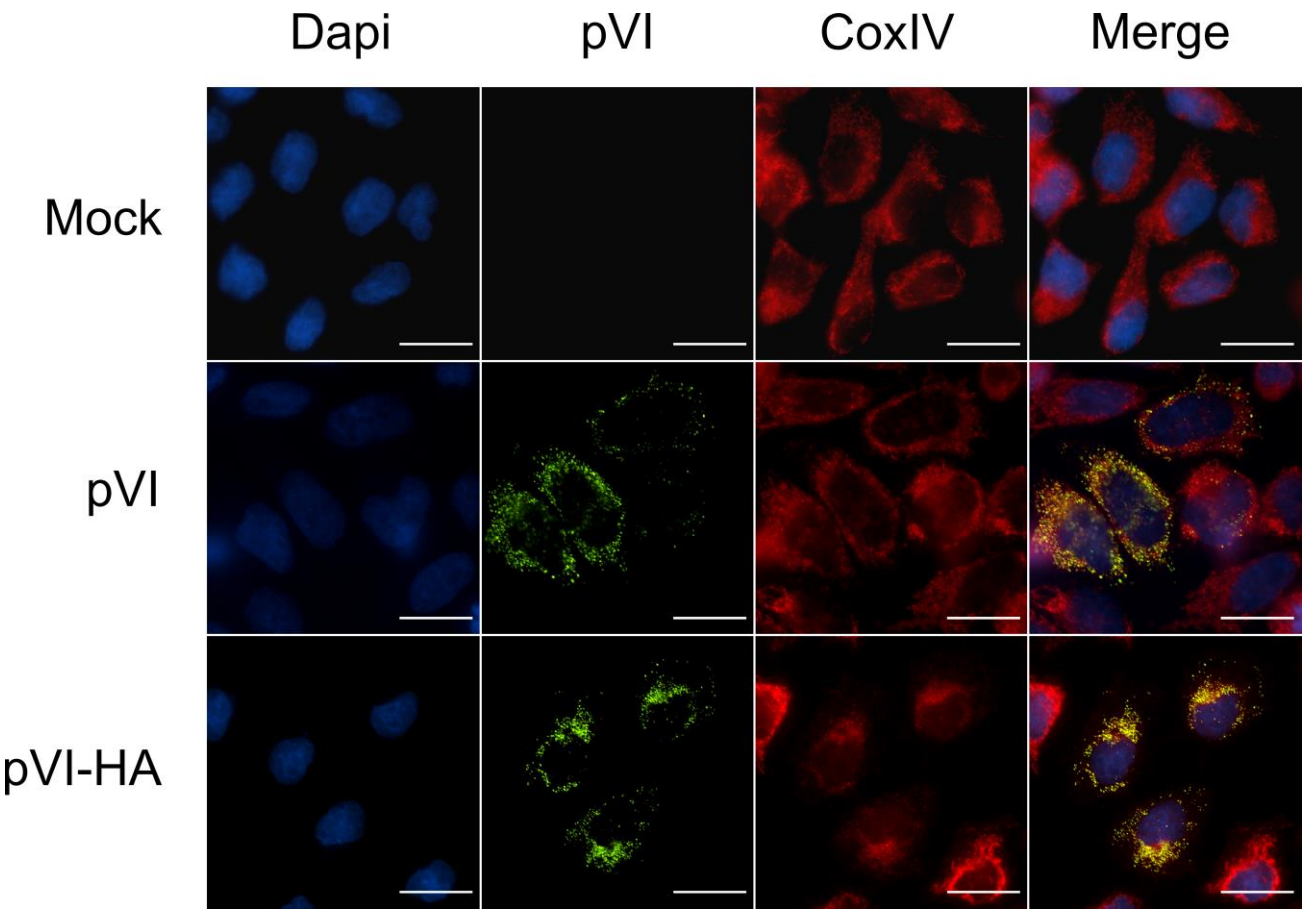

Figure 11. HAdV-C5 pVI protein implicates mitochondrial localization. HeLa-Kyoto cells were transfected with plasmids expressing the pVI (wt) and pVI (wt)-HA proteins. 24 hours post transfection the cells were fixed and permeabilized, followed by straining of the cells with antibodies targeting the pVI (Green) and CoxIV (Red) proteins. The latter acts as the mitochondrial marker. Dapi staining is depicted in blue. The cells were analyzed at 60x magnification. Scale bars represent 20 µm.

For increased resolution, and to investigate the mitochondrial interaction of pVI in living cells, the proteins localization was visualized with confocal microscopy. Live cell imaging was done in a collaboration with Dr. Olof Idevall and Styliani Panagiotou at the Department of Medical Cell Biology at Uppsala university. For this purpose, the pVI (wt), pVI (L40Q), pVI (34-239) and pVI (55-239) cDNAs (Figure 2) were cloned into plasmids expressing a GFP-pVI fusion protein, with the green fluorescent protein (GFP) fused into the N-terminal end of the pVI proteins. Hela-Kyoto cells were co-transfected with the GFP-pVI plasmids

and fluorescent tag containing mApple-Tomm20 or mCherry-Rab5 expressing plasmids. The Tomm20 and Rab5 proteins acted as mitochondrial or endosomal markers, respectively. Confocal microscopy revealed a striking co-localization of the GFP-tagged wild type pVI protein with Tomm20, located on the outer mitochondrial membrane (Figure 12). The GFP-tagged mature form of pVI (34-239) showed a weak co-localization with Tomm20, however expression levels of the pVI (34-239) protein were rather low (Figure 12). Interestingly, the pVI mutant lacking the amphipathic helix (55-239) and the L40Q point mutant exhibited a clear cytosolic and nuclear localization when fused with a GFP on the N-terminal, where co-localization with Tomm20 was absent (Figure 12). This observation contradicts the localization of these two mutants seen in the biochemical fractionation, where both proteins were still found localized into the mitochondrial fraction (Figures 7C and 8B). As pVI mediates the endosomal escape upon virion entry, the co-localization of pVI with endosomes was also studied. Interestingly, pVI (wt), pVI (34-239) and pVI (L40Q) produced distinctly dotted structures, initially thought to be endosomes (Figure 12). Surprisingly, the dotted structures of the pVI constructs show limited association with Rab5, an early endosomal marker (Figure 12) suggesting that the protein is not targeting endosomes when transiently expressed as the GFP fusion protein. Together, both immunofluorescence and confocal microscopy analysis revealed a strong localization of the wild-type pVI protein to mitochondria.

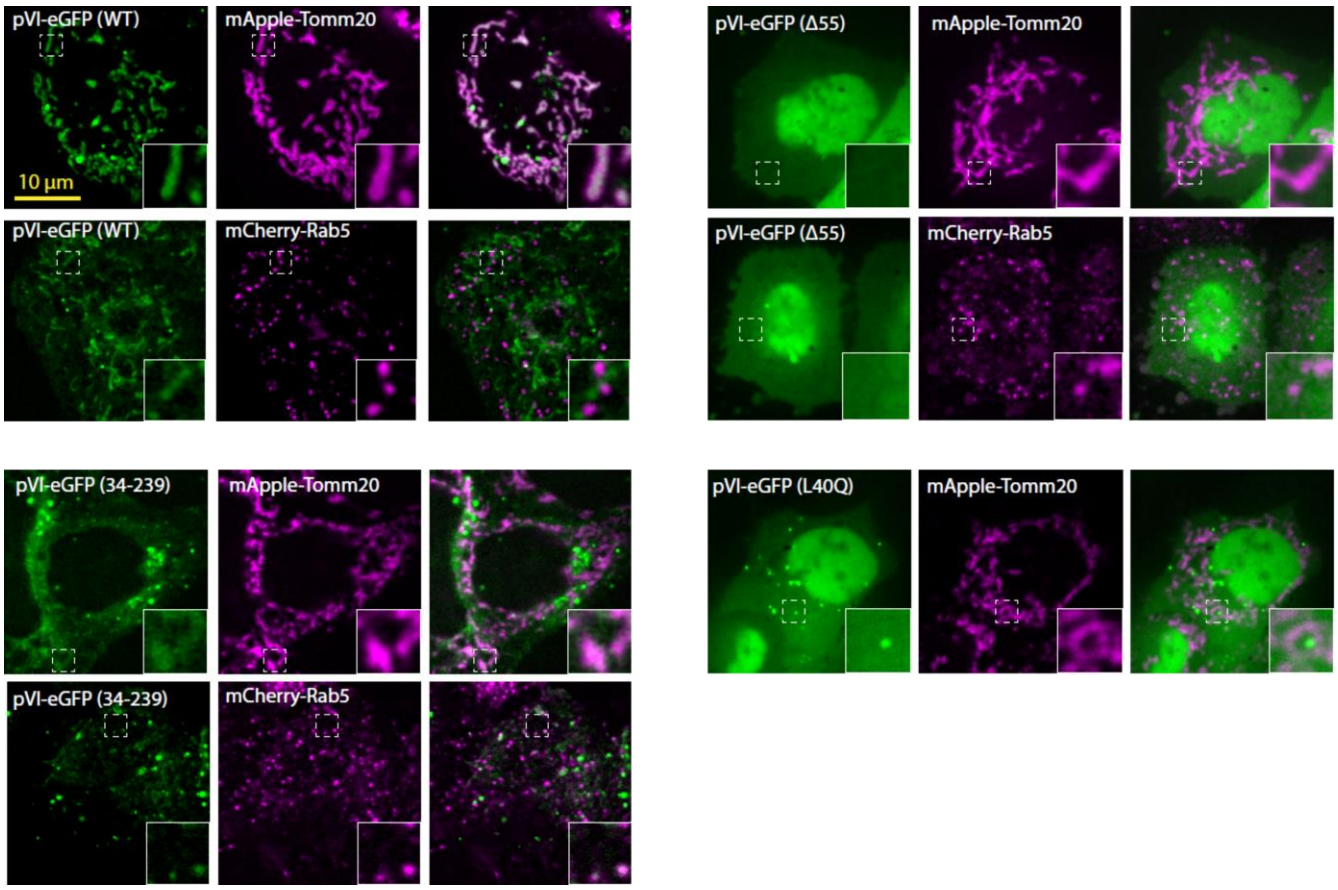

Figure 12. HAdV-C5 pVI protein co-localizes with mitochondria. HeLa-Kyoto were transfected with plasmids expressing the GFP-pVI (wt), GFP-pVI (L40Q), GFP-pVI (34-239), and GFP-pVI (55-239) proteins with co-transfection of either mApple-Tomm20 or mCherry-Rab5 expressing plasmids. Tomm20 and Rab5 acted as the mitochondrial or endosomal marker, respectively. 24 hours post transfection the live cells were analyzed using confocal microscopy at 100x magnification. Scale bar represents 10 µm.

The HAdV-C5 pVI protein and L40Q mutant hyperpolarize the mitochondrial membrane.
The membrane disruptive properties of pVI can potentially be linked to consequences other than mtDNA release. One such consequence is the alteration of the mitochondrial membrane potential which can lead to changes in ATP production or calcium exchange. Mitochondrial membrane potential measurement was done in a continued collaboration with Dr. Olof Idevall and Styliani Panagiotou. To this end, HeLa-Kyoto cells were transfected with pVI (wt)-HA and pVI (L40Q)-HA expressing plasmids. The expected transfection efficiency for these cells is 80-90 %. 24 hours post transfection the cells were stained with TMRM dye. This dye accumulates in active mitochondria and gives off a bright fluorescent signal in cells with a functional resting membrane potential. The fluorescent signal was measured using epifluorescence microscopy. After resting potential measurement, the mitochondrial membrane was depolarized with FCCP. The measured membrane potential was normalized to the lowest values achieved upon FCCP addition, which assumes that the membrane potential has diminished. Interestingly, both the pVI (wt)-HA and pVI (L40Q)-HA proteins hyperpolarized the mitochondrial membrane to a similar extent (Figure 13). This finding implies that the pVI protein might remodel different mitochondrial properties apart from inducing mtDNA release into the cytosol.

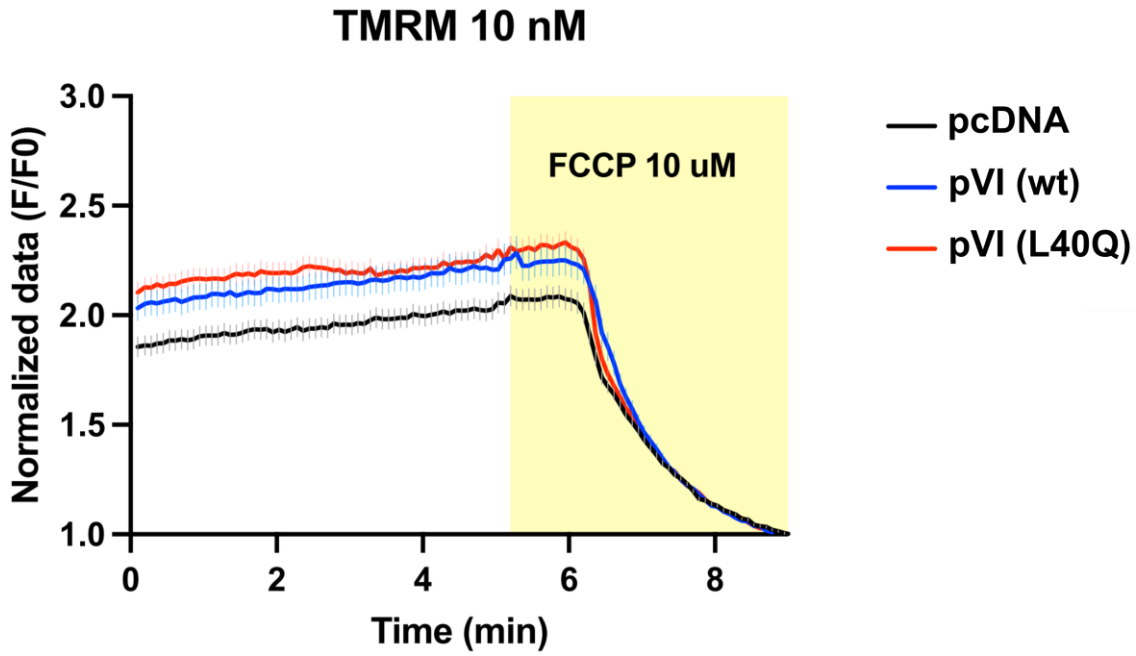

Figure 13. The pVI (wt)-HA protein and pVI (L40Q)-HA mutant hyperpolarize the mitochondrial membrane. HeLa-Kyoto cells were transfected with plasmids expressing the pVI (wt)-HA and pVI (L40Q)-HA proteins. 24 hours post transfection the cells were stained with 10 nM TMRM, followed by mitochondrial resting potential measurement with epifluorescence microscopy in a scope of approximately 50 cells. After 5 minutes of TMRM infusion, the cells were depolarized with 10 µM FCCP for 5 minutes. The resting potential data was normalized to the lowest fluorescence value obtained upon FCCP addition, which assumes that the membrane potential has diminished.

Discussion

Research continuously unveils viral proteins that modulate mitochondrial functions, including mitochondrial DNA (mtDNA) dynamics. Notably, recent studies demonstrated that several RNA viruses, such as influenza A and dengue virus, can induce the release of mtDNA into the cytosol (Li et al., 2020; Moriyama et al., 2019; Sun et al., 2017). In addition, mtDNA released upon viral infections has been shown to act as a potent signaling molecule that activates innate immune receptors (West et al., 2011). However, the detailed molecular mechanism behind virus mediated mitochondrial modulations and mtDNA release have remained largely unclear.

The present thesis together with the preliminary data from Dr. Kwangchol Mun (Mun, 2019) shows that HAdV-C5, a DNA virus can induce the release of mtDNA into the cytosol of the infected cells (Figure 4, 5 and 6). In addition, the virus induced mtDNA release correlates to the late pVI protein expression (Figure 5). In line with this observation, the pVI protein alone is sufficient in inducing the release of mtDNA, dependent largely on the proteins N-terminal amphipthatic helix (Figure 7 and 8). Furthermore, biochemical fractionation experiments showed a clear accumulation of pVI in the mitochondrial fraction (Figure 7 and 8). Immunofluorescence and confocal microscopy confirmed that pVI co-localizes with mitochondrial proteins (Figure 11 and 12). Apart from mtDNA release, expression of the pVI protein also influences the mitochondrial membrane potential, suggesting that the protein may interfere with several mitochondrial functions (Figure 13).

A major challenge in this study was the optimization of the methods to express the pVI protein and isolate the cytosolic mtDNA. As shown in Figure 7A the non-codon optimized cDNAs of pVI expressed low proteins levels. Therefore, the pVI protein (Figure 2) cDNAs were codon-optimized at GenScript Biotech. In codon-optimization, factors such as GC content, codon usage, RNA splicing sites and cis-acting mRNA destabilization motifs are adjusted for maximum protein expression. This approach drastically increased pVI detection with the anti-HA and anti-pVI antibodies, enabling a clear biochemical analysis of the protein. Additionally, detection of mtDNA from cytosolic fractions with an NaOH based DNA isolation approach led to large variations in the DNA CT values within technical replicates when analyzed with the qPCR approach. To address this problem, the cytosolic fractions were extensively pre-cleared by centrifugation for increased fraction purity. Subsequently, the cytosolic mtDNA was isolated with a specific kit (see Materials and Methods section) designed to bind DNA up to 10 kbp. Together, these adjustments enabled reproducible detection of cytosolic mtDNA in HAdV-C5-infected and pVI-transfected cells.

Microscopy and biochemical results in this study reveal that the wild-type pVI protein consistently targets and localizes to mitochondria, which has not been observed before. Recent pVI research focused mainly on the mature protein (34-239) in connection to capsid disassembly or endosome membrane lysis with little focus on the full-length protein (wt, 1-250) produced in the late phase of infection (Hernando-Pérez et al., 2020; Wiethoff and Nemerow, 2015). This is the first study that used a biochemical fractionation approach to reveal how the protein is processed and localized in different subcellular fractions.

In the biochemical fractionation experiments pVI was mainly detected as truncated variants, several kDa lower than the full-length protein (Figure 7C). Notably, these truncated versions were only seen in the mitochondrial fraction. Knockdown of the translocase of the outer mitochondrial membrane subunit 40 (Tomm40) induced less pVI protein accumulation and processing in the mitochondrial fraction (Figure 10B). However, enough pVI was still present in the mitochondrial fraction to induce mtDNA release (Figure 10B). This finding suggests that the protein may enter the mitochondrial interior through the outer mitochondrial membrane. Endogenous proteins targeted to mitochondria commonly contain an N-terminal

mitochondrial targeting sequence (MTS) (Endo and Kohda, 2002). This MTS is comprised of amino acids that exhibit the structure of an amphipathic helix (Cooper, 2000). The physiochemical properties of the amphipathic helix are recognized by the Tomm20 and Tomm22 receptors which initiate protein translocation through the Tomm40 transport channel (Endo and Kohda, 2002). For instance, the unconventional amphipathic helix present at the C-terminal of the IAV PB1-F2 protein targets the protein into the mitochondria (Gibbs et al., 2003). Transport of proteins through the mitochondrial membrane is usually followed by protein processing via the mitochondrial processing peptidases (Backes and Herrmann, 2017). The N-terminal amphipathic helix of pVI could act as a mitochondrial targeting sequence in addition to or instead of mediating outer mitochondrial membrane lysis directly. Upon pVI protein translocation through the outer membrane the protein may be processed by various mitochondrial proteases, possibly explaining why pVI appears in truncated forms during biochemical analysis. In addition, the pVI (55-239) mutant, lacking the amphipathic helix, exhibits significantly less mitochondrial localization in biochemical and microscopic analysis (Figure 7 and 12). This supports the role of the amphipathic helix for mitochondrial targeting. Furthermore, Figure 13 suggests that the pVI protein induced mitochondrial membrane hyperpolarization which applies to the inner mitochondrial membrane where ATP production occurs. This finding also suggests that protein localizes into mitochondria, rather than associating to the outside.

Co-expression of the E1B-19k and pVI proteins blocked the pVI-mediated mtDNA release (Figure 9A). Additionally, elimination of the Bax and Bak proteins by an siRNA approach led to a lower accumulation of cyto-mtDNA upon pVI overexpression (Figure 10A). These findings suggest an interaction of the pVI protein with the Bax and Bak mediated MOMP, which has been shown to induce mtDNA efflux into the cytosol (McArthur et al., 2018). Accumulation of the pVI protein in the mitochondrial inter membrane space or matrix might induce extensive levels of mitochondrial stress. This stress might consequently activate the Bax and Bak proteins to eliminate dysfunctional mitochondria. Alternatively, pVI might directly associate with the Bax and Bak proteins or disrupt the inner mitochondrial membrane through its membrane lytic activity. From the HAdV infection perspective, E1B-19k binds and sequesters the endogenous Bax and Bak proteins in the early phase of infection to prevent apoptosis (Han et al., 1996). Furthermore, this function might also block early interactions of the mature pVI protein with Bax and Bak upon virus entry. Figure 7A implicates that the mature pVI (34-239), present in the infecting viral capsid can also induce mtDNA release into the cytosol. During the late phase of infection, wild-type pVI is produced in a massive amount, possibly overcoming the suppressive effect E1B-19k to subsequently influence mitochondrial membrane and mtDNA dynamics. Interestingly, transient co-overexpression of the pVI proteins led to significantly lower accumulation of E1B-19k protein (Figure 9B). Hypothetically, this observation may indicate that the pVI protein targets E1B-19k for proteolytic degradation. The pVI protein is known to bind the E3-protein ubiquitin ligase Nedd4 in a PPxY motif-dependent manner (Wodrich et al., 2010). Hence, it is possible that the pVI recruited Nedd4 induces proteasomal degradation of the E1B-19k protein.

The L40Q point mutation in the pVI proteins amphipathic helix led to less cytosolic mtDNA when compared to the wild-type protein (Figure 8 A and C). How exactly this mutation impairs the role of the protein remains unclear. It was firstly proposed that this mutation lowers the association of the protein with the mitochondrial membrane, similar to its effect on endosomal membranes (Moyer et al., 2011). Biochemical analysis revealed that the L40Q mutant is expressed to the same extent as the wild-type protein truncated in the mitochondrial fraction, while inducing less cyto-mtDNA (Figure 8 B and D). This suggests that the altered amphipathic helix of the L40Q mutant is sufficient to target the protein into mitochondria. Additionally, since the anti-HA antibody detected the C-terminally fused HA epitope on the full-length proteins but failed to detect the truncated proteins located in the mitochondrial fraction (Figure 7C) suggests that the pVI protein is processed at the C-terminus upon associating with mitochondria. This implies that the N-terminal amphipathic helix is still functional inside mitochondria and could possibly

disrupt the inner mitochondrial membrane, explaining why the L40Q with less membrane lytic affinity induced less cyto-mtDNA.

The present thesis elucidated that the pVI protein is pivotal in the HAdV-C5 induced mtDNA release. However, it remains enigmatic why HAdV-C5 infection causes this release. One explanation would be that the mtDNA is released to induce the innate immune system in host cells as an alternative anti-viral response. In the case of IAV and dengue virus infection, released mtDNA activates the cGAS-STING and TLR9 pattern recognition receptors (PRRs), respectively. Therefore, both viruses effectively upregulate the IFN-β gene expression (Lai et al., 2018; Moriyama et al., 2019). This outcome could logically be applied to the HAdV induced mtDNA release, although the viral dsDNA is recognized by PRRs such as cGAS or TLR9 as well. Alternatively, release of mtDNA in HAdV-C5 infection might support efficient release of the virus from host cells. Mun (2019) speculated that mtDNA might be recognized as a signal to facilitate viral release from infected cells. In addition to this speculation, the mtDNA release in HAdV infection is probably related to Bax- and Bak- induced MOMP. This could initiate apoptotic signaling pathways, and consequently lead to fragmentation of cells which would be beneficial for mature virus particles, in the sense that this process can facilitate virus release.

Further studies are needed to determine if and how pVI interacts with mitochondrial proteins to induce mtDNA release or disruption of mitochondrial membranes. In addition to mtDNA, it would be interesting to study whether mitochondrial double-stranded RNA is released into the cytosol of HAdV infected cells. Double-stranded RNA can also act as a potent signaling molecule that activates RNA sensitive PRRs. In connection, the association of cytosolic mtDNA to immune receptors such as cGAS or TLR9 would be an important investigation to study the antiviral response in HAdV infected cells. This should optimally be studied in immune cell lines, such as THP-1 cells, as these cells express the TLR9 receptor. Additionally, it would be important to determine whether the pVI protein’s interaction with Bax and Bak can induce apoptosis. In conclusion, this thesis revealed that another well-known virus, HAdV-C5, can interact with and modulate mitochondrial DNA and membrane dynamics through the viral pVI protein.

Acknowledgements

I would like to thank my supervisor Dr. Tanel Punga for sharing his extensive knowledge in molecular virology and introducing me to the laboratory techniques needed to study the pVI protein. Your support and your discussions were invaluable in accomplishing this thesis. Furthermore, I want to thank Dr. Olof Idevall and Styliani Panagiotou for taking their time by performing and showing me how confocal microcopy and membrane potential measurements are done. I want to thank my classmate Katharina Julia Kases for introducing me to the basics of immunofluorescence microscopy. I also want to give my gratitude and appreciation to my office colleagues who have always been helpful and created a fun working environment. Lastly, I want to express my gratefulness for Dr. Kwangchol Mun who unlocked my passion for research in molecular virology. You inspired me and I feel honored to continue the study you started to achieve my MSc.

References

Acheson, N.H., 2011. Fundamentals of molecular virology, 2nd ed. ed. John Wiley & Sons, Hoboken, NJ.

Alberts, B. (Ed.), 2008. Molecular biology of the cell, 5th ed. ed. Garland Science, New York.

Anand, S.K., Tikoo, S.K., 2013. Viruses as Modulators of Mitochondrial Functions. Advances in Virology 2013, 1–17. https://doi.org/10.1155/2013/738794

Backes, S., Herrmann, J.M., 2017. Protein Translocation into the Intermembrane Space and Matrix of Mitochondria: Mechanisms and Driving Forces. Front Mol Biosci 4, 83. https://doi.org/10.3389/fmolb.2017.00083

Berk, A.J., 2016. Discovery of RNA splicing and genes in pieces. Proc Natl Acad Sci USA 113, 801–805. https://doi.org/10.1073/pnas.1525084113

Berk, A.J., 2005. Recent lessons in gene expression, cell cycle control, and cell biology from adenovirus. Oncogene 24, 7673–7685. https://doi.org/10.1038/sj.onc.1209040

Boguszewska, K., Szewczuk, M., Kaźmierczak-Barańska, J., Karwowski, B.T., 2020. The Similarities between Human Mitochondria and Bacteria in the Context of Structure, Genome, and Base Excision Repair System. Molecules 25, 2857. https://doi.org/10.3390/molecules25122857

Cady, S.D., Luo, W., Hu, F., Hong, M., 2009. Structure and Function of the Influenza A M2 Proton Channel. Biochemistry 48, 7356–7364. https://doi.org/10.1021/bi9008837

Campbell, N.A., Reece, J.B., 2015. Biology: a global approach, 10. ed., global ed. ed. Pearson, Boston.

Chinnery, P.F., 1993. Mitochondrial Disorders Overview, in: Adam, M.P., Ardinger, H.H., Pagon, R.A., Wallace, S.E., Bean, L.J., Mirzaa, G., Amemiya, A. (Eds.), GeneReviews®. University of Washington, Seattle, Seattle (WA).

Cooper, G.M., 2000. The cell: a molecular approach, 2. ed. ed. ASM Press [u.a.], Washington, DC.

Corcoran, J.A., Saffran, H.A., Duguay, B.A., Smiley, J.R., 2009. Herpes Simplex Virus UL12.5 Targets Mitochondria through a Mitochondrial Localization Sequence Proximal to the N Terminus. JVI 83, 2601–2610. https://doi.org/10.1128/JVI.02087-08

Endo, T., Kohda, D., 2002. Functions of outer membrane receptors in mitochondrial protein import. Biochim Biophys Acta 1592, 3–14. https://doi.org/10.1016/s0167-4889(02)00259-8

García-Montero, C., Fraile-Martínez, O., Bravo, C., Torres-Carranza, D., Sanchez-Trujillo, L., Gómez-Lahoz, A.M., Guijarro, L.G., García-Honduvilla, N., Asúnsolo, A., Bujan, J., Monserrat, J., Serrano, E., Álvarez-Mon, M., De León-Luis, J.A., Álvarez-Mon, M.A., Ortega, M.A., 2021. An Updated Review of SARS-CoV-2 Vaccines and the Importance of Effective Vaccination Programs in Pandemic Times. Vaccines 9, 433. https://doi.org/10.3390/vaccines9050433

Garcia-Moure, M., Martinez-Vélez, N., Patiño-García, A., Alonso, M.M., 2017. Oncolytic adenoviruses as a therapeutic approach for osteosarcoma: A new hope. Journal of Bone Oncology 9, 41–47. https://doi.org/10.1016/j.jbo.2016.12.001
Gibbs, J.S., Malide, D., Hornung, F., Bennink, J.R., Yewdell, J.W., 2003. The Influenza A Virus PB1-F2 Protein Targets the Inner Mitochondrial Membrane via a Predicted Basic Amphipathic Helix That Disrupts Mitochondrial Function. JVI 77, 7214–7224. https://doi.org/10.1128/JVI.77.13.7214-7224.2003
Gorman, G.S., Chinnery, P.F., DiMauro, S., Hirano, M., Koga, Y., McFarland, R., Suomalainen, A., Thorburn, D.R., Zeviani, M., Turnbull, D.M., 2016. Mitochondrial diseases. Nat Rev Dis Primers 2, 16080. https://doi.org/10.1038/nrdp.2016.80
Han, J., Sabbatini, P., Perez, D., Rao, L., Modha, D., White, E., 1996. The E1B 19K protein blocks apoptosis by interacting with and inhibiting the p53-inducible and death-promoting Bax protein. Genes & Development 10, 461–477. https://doi.org/10.1101/gad.10.4.461
Hernando-Pérez, M., Martín-González, N., Pérez-Illana, M., Suomalainen, M., Condezo, G.N., Ostapchuk, P., Gallardo, J., Menéndez, M., Greber, U.F., Hearing, P., de Pablo, P.J., San Martín, C., 2020. Dynamic competition for hexon binding between core protein VII and lytic protein VI promotes adenovirus maturation and entry. Proc Natl Acad Sci U S A 117, 13699–13707. https://doi.org/10.1073/pnas.1920896117
Hierholzer, J.C., 1992. Adenoviruses in the immunocompromised host. Clin. Microbiol. Rev. 5, 262–274. https://doi.org/10.1128/CMR.5.3.262
Inturi, R., Thaduri, S., Punga, T., 2013. Adenovirus Precursor pVII Protein Stability Is Regulated By Its Propeptide Sequence. PLoS ONE 8, e80617. https://doi.org/10.1371/journal.pone.0080617
Kalkavan, H., Green, D.R., 2018. MOMP, cell suicide as a BCL-2 family business. Cell Death Differ 25, 46–55. https://doi.org/10.1038/cdd.2017.179
Khanal, S., Ghimire, P., Dhamoon, A., 2018. The Repertoire of Adenovirus in Human Disease: The Innocuous to the Deadly. Biomedicines 6, 30. https://doi.org/10.3390/biomedicines6010030
Ladoukakis, E.D., Zouros, E., 2017. Evolution and inheritance of animal mitochondrial DNA: rules and exceptions. J of Biol Res-Thessaloniki 24, 2. https://doi.org/10.1186/s40709-017-0060-4
Lai, J., Wang, M., Huang, C., Wu, C., Hung, L., Yang, C., Ke, P., Luo, S., Liu, S., Ho, L., 2018. Infection with the dengue RNA virus activates TLR9 signaling in human dendritic cells. EMBO Rep 19. https://doi.org/10.15252/embr.201846182
Lamphier, M.S., Sirois, C.M., Verma, A., Golenbock, D.T., Latz, E., 2006. TLR9 and the Recognition of Self and Non-Self Nucleic Acids. Annals of the New York Academy of Sciences 1082, 31–43. https://doi.org/10.1196/annals.1348.005
Lee, S.R., Han, J., 2017. Mitochondrial Nucleoid: Shield and Switch of the Mitochondrial Genome. Oxidative Medicine and Cellular Longevity 2017, 1–15. https://doi.org/10.1155/2017/8060949
Li, M.X., Dewson, G., 2015. Mitochondria and apoptosis: emerging concepts. F1000Prime Rep 7. https://doi.org/10.12703/P7-42
Li, S., Li, H., Zhang, Y.-L., Xin, Q.-L., Guan, Z.-Q., Chen, X., Zhang, X.-A., Li, X.-K., Xiao, G.-F., Lozach, P.-Y., Cui, J., Liu, W., Zhang, L.-K., Peng, K., 2020. SFTSV Infection Induces BAK/BAX-Dependent Mitochondrial DNA Release to Trigger NLRP3 Inflammasome Activation. Cell Reports 30, 4370-4385.e7. https://doi.org/10.1016/j.celrep.2020.02.105
Lomonosova, E., Subramanian, T., Chinnadurai, G., 2005. Mitochondrial localization of p53 during adenovirus infection and regulation of its activity by E1B-19K. Oncogene 24, 6796–6808. https://doi.org/10.1038/sj.onc.1208836
Martínez-Campos, C., Burguete-García, A.I., Madrid-Marina, V., 2017. Role of TLR9 in Oncogenic Virus-Produced Cancer. Viral Immunology 30, 98–105. https://doi.org/10.1089/vim.2016.0103
Matthews, D.A., Russell, W.C., 1998. Adenovirus core protein V interacts with p32--a protein which is associated with both the mitochondria and the nucleus. Journal of General Virology 79, 1677–1685. https://doi.org/10.1099/0022-1317-79-7-1677

McArthur, K., Whitehead, L.W., Heddleston, J.M., Li, L., Padman, B.S., Oorschot, V., Geoghegan, N.D., Chappaz, S., Davidson, S., San Chin, H., Lane, R.M., Dramicanin, M., Saunders, T.L., Sugiana, C., Lessene, R., Osellame, L.D., Chew, T.-L., Dewson, G., Lazarou, M., Ramm, G., Lessene, G., Ryan, M.T., Rogers, K.L., van Delft, M.F., Kile, B.T., 2018. BAK/BAX macropores facilitate mitochondrial herniation and mtDNA efflux during apoptosis. Science 359, eaao6047. https://doi.org/10.1126/science.aao6047

Moriyama, M., Koshiba, T., Ichinohe, T., 2019. Influenza A virus M2 protein triggers mitochondrial DNA-mediated antiviral immune responses. Nat Commun 10, 4624. https://doi.org/10.1038/s41467-019-12632-5

Moriyama, M., Nagai, M., Maruzuru, Y., Koshiba, T., Kawaguchi, Y., Ichinohe, T., 2020. Influenza Virus-Induced Oxidized DNA Activates Inflammasomes. iScience 23, 101270. https://doi.org/10.1016/j.isci.2020.101270

Moyer, C.L., Wiethoff, C.M., Maier, O., Smith, J.G., Nemerow, G.R., 2011. Functional Genetic and Biophysical Analyses of Membrane Disruption by Human Adenovirus. Journal of Virology 85, 2631–2641. https://doi.org/10.1128/JVI.02321-10

Mun, K., 2019. Human adenovirus – host cell interplay: The role of the cellular zinc finger proteins and mitochondrial DNA.

Muta, T., Kang, D., Kitajima, S., Fujiwara, T., Hamasaki, N., 1997. p32 Protein, a Splicing Factor 2-associated Protein, Is Localized in Mitochondrial Matrix and Is Functionally Important in Maintaining Oxidative Phosphorylation. Journal of Biological Chemistry 272, 24363–24370. https://doi.org/10.1074/jbc.272.39.24363

Osellame, L.D., Blacker, T.S., Duchen, M.R., 2012. Cellular and molecular mechanisms of mitochondrial function. Best Practice & Research Clinical Endocrinology & Metabolism 26, 711–723. https://doi.org/10.1016/j.beem.2012.05.003

Riley, J.S., Tait, S.W., 2020. Mitochondrial DNA in inflammation and immunity. EMBO Rep 21. https://doi.org/10.15252/embr.201949799

Rodríguez-Nuevo, A., Zorzano, A., 2019. The sensing of mitochondrial DAMPs by non-immune cells. CST 3, 195–207. https://doi.org/10.15698/cst2019.06.190

Roger, A.J., Muñoz-Gómez, S.A., Kamikawa, R., 2017. The Origin and Diversification of Mitochondria. Current Biology 27, R1177–R1192. https://doi.org/10.1016/j.cub.2017.09.015

Shimada, K., Crother, T.R., Karlin, J., Dagvadorj, J., Chiba, N., Chen, S., Ramanujan, V.K., Wolf, A.J., Vergnes, L., Ojcius, D.M., Rentsendorj, A., Vargas, M., Guerrero, C., Wang, Y., Fitzgerald, K.A., Underhill, D.M., Town, T., Arditi, M., 2012. Oxidized Mitochondrial DNA Activates the NLRP3 Inflammasome during Apoptosis. Immunity 36, 401–414. https://doi.org/10.1016/j.immuni.2012.01.009

Siekevitz, P., 1957. Powerhouse of the Cell. Sci Am 197, 131–144. https://doi.org/10.1038/scientificamerican0757-131

Sun, B., Sundström, K.B., Chew, J.J., Bist, P., Gan, E.S., Tan, H.C., Goh, K.C., Chawla, T., Tang, C.K., Ooi, E.E., 2017. Dengue virus activates cGAS through the release of mitochondrial DNA. Sci Rep 7, 3594. https://doi.org/10.1038/s41598-017-03932-1

Tiku, V., Tan, M.-W., Dikic, I., 2020. Mitochondrial Functions in Infection and Immunity. Trends in Cell Biology 30, 263–275. https://doi.org/10.1016/j.tcb.2020.01.006

Ugai, H., Dobbins, G.C., Wang, M., Le, L.P., Matthews, D.A., Curiel, D.T., 2012. Adenoviral protein V promotes a process of viral assembly through nucleophosmin 1. Virology 432, 283–295. https://doi.org/10.1016/j.virol.2012.05.028

Verrier, E.R., Langevin, C., 2021. Cyclic Guanosine Monophosphate–Adenosine Monophosphate Synthase (cGAS), a Multifaceted Platform of Intracellular DNA Sensing. Front. Immunol. 12, 637399. https://doi.org/10.3389/fimmu.2021.637399

West, A.P., Shadel, G.S., Ghosh, S., 2011. Mitochondria in innate immune responses. Nat Rev Immunol 11, 389–402. https://doi.org/10.1038/nri2975

Wiethoff, C.M., Nemerow, G.R., 2015. Adenovirus membrane penetration: Tickling the tail of a sleeping dragon. Virology 479–480, 591–599. https://doi.org/10.1016/j.virol.2015.03.006
Wodrich, H., Henaff, D., Jammart, B., Segura-Morales, C., Seelmeir, S., Coux, O., Ruzsics, Z., Wiethoff, C.M., Kremer, E.J., 2010. A Capsid-Encoded PPxY-Motif Facilitates Adenovirus Entry. PLoS Pathog 6, e1000808. https://doi.org/10.1371/journal.ppat.1000808
Youle, R.J., van der Bliek, A.M., 2012. Mitochondrial Fission, Fusion, and Stress. Science 337, 1062–1065. https://doi.org/10.1126/science.1219855
Zhang, Y., Bergelson, J.M., 2005. Adenovirus receptors. J Virol 79, 12125–12131. https://doi.org/10.1128/JVI.79.19.12125-12131.2005